Flood, R.D., Piper, D.J.W., Klaus, A., and Peterson, L.C. (Eds.), 1997
Proceedings of the Ocean Drilling Program, Scientific Results, Vol. 155

2. SANDY TURBIDITE SUCCESSIONS AT THE BASE OF CHANNEL-LEVEE SYSTEMS OF THE AMAZON FAN REVEALED BY FMS LOGS AND CORES: UNRAVELING THE FACIES ARCHITECTURE OF LARGE SUBMARINE FANS[1]

Carlos Pirmez,[2] Richard N. Hiscott,[3] and John D. Kronen, Jr.[4]

ABSTRACT

Continuous bed-by-bed descriptions of thick, sand-rich turbidite successions drilled at five sites on the Amazon Fan have been prepared using a combination of Formation MicroScanner (FMS) and geophysical wireline logs. FMS images enable a complete lithologic section to be derived at Sites 931, 935, 936, 944, and 946 over intervals of poor core recovery up to several tens of meters thick, characterized as high-amplitude reflection packets (HARPs) in the seismic data. On the middle fan, HARP deposition coincides in time with the initiation of a new channel segment after channel bifurcation. Toward the lower fan, HARP units tend to stack directly on top of each other, as overbank deposits thin downfan; these HARP units probably contain deposits formed at the mouths of channels.

The turbidite successions within the HARP intervals include sand bodies 5–25 m thick formed of sand beds 0.1–4 m thick. These sand bodies correlate with episodes of channel bifurcation on the middle fan. Most beds thicker than ~1 m contain mud clasts, interpreted to result from upslope levee erosion and channel entrenchment after channel bifurcation. On the lower fan, bed clusters and sets of amalgamated beds form sand bodies as thick as 50 m, with individual beds often exceeding 3 m in thickness and containing abundant mud clasts. Most bed clusters show no apparent trends in bed thickness, although a few clusters show clear thickening-upward trends interpreted to represent channel mouth progradation.

Other studies suggest that, for turbidites, the number of beds whose thickness is greater than T is proportional to T^{-B}, where B is a positive exponent. The scaling exponent required to fit the Amazon Fan bed-thickness distributions is different for beds thinner and thicker than about 0.35 m. This difference is attributed to either selective removal, by erosion, of beds thinner than ~0.35 m, or greater confinement, by seafloor morphology, of flows that deposited such thin beds on the fan surface. The flows that deposited beds thicker than 0.35 m in HARP units were apparently able to freely spread in the interlevee area.

The so-called mud-rich Amazon Fan contains thick sheet-like units indistinguishable in facies and sand content from many ancient mud/sand-rich successions described by field geologists. Although it remains true that small fans at convergent and strike-slip plate boundaries are potentially good analogs for such ancient deposits, larger channel-levee–dominated systems that periodically supply sand to interchannel depressions following avulsions also need to be considered.

INTRODUCTION

The Amazon Fan is a large cone-shaped deposit of terrigenous sediments derived from the Amazon River drainage basin. The fan succession reaches a thickness of ~7 km near the northeast Brazil shelf break. Its age is middle Miocene and younger (Castro et al., 1978). The surface of the fan is covered by a distributary network of meandering channels that has been mapped with SeaBeam swath bathymetry and GLORIA side-scan sonar (Damuth et al., 1988; Flood et al., 1991). High-resolution seismic data show that these meandering channels are bounded by high natural levees and are perched atop their own overbank deposits (i.e., the channel-levees and often the channel talweg are elevated above the surrounding fan surface; Pirmez and Flood, 1995). Channel-levees result from the vertical and lateral expansion of turbidity currents traveling through the meandering channels (Hiscott et al., this volume). The aggrading channel and overbank deposits often bifurcate. Such bifurcation is caused by levee breaching and avulsion, leaving one branch of the channel inactive and initiating the formation of a new channel downslope. As a result, the fan builds laterally and vertically through the stacking and overlapping of these lens-shaped, channel-overbank deposits.

The channel patterns on the Amazon Fan are seen on other so-called mud-rich fans such as the Indus Fan (McHargue, 1991; Droz and Bellaiche, 1991), Mississippi Fan (Weimer, 1990), Rhône Fan (Droz and Bellaiche, 1985), Magdalena Fan (Pirmez et al., 1990), and Zaire Fan (Droz et al., 1996). Although these submarine fans have all been acoustically imaged to varying degrees of detail, sampling of the fan sediments generally has been limited to the upper 10 m, and the lithofacies and/or sedimentary processes associated with the acoustic units observed on seismic reflection data are conjectural (e.g., Weimer, 1990; Manley and Flood, 1988). Prior to Ocean Drilling Program (ODP) Leg 155, only the Mississippi Fan was drilled with the specific objective of deep sampling of submarine fan channel-levee deposits, which allowed characterization of the sediments associated with the youngest channel system on that fan, as well as other seismic units (Bouma, Coleman, Meyer, et al., 1986). Only a limited logging program was available on the Mississippi Fan, and the coring techniques employed produced limited recovery and severely disturbed the original structures of the unconsolidated sediments at some sites. More recently, during Leg 116, turbidites were drilled at the distal edge of the Indus Fan (Cochran, Stow, Auroux, et al., 1989).

During Leg 155, 34 holes were drilled at 17 sites (Fig. 1A). At several sites, the uppermost ~100 m of the succession was cored several times with the advanced piston corer (APC) to ensure sufficient sediment for detailed shore-based studies. If one ignores all but a single penetration of this upper part of the sediment column, the average core recovery at the five sites considered in this paper (Sites 931, 935, 936, 944, and 946), from the seafloor to the depth of greatest penetration, was 65%. Core recovery was high in mud-rich levee deposits, particularly from 0 to 100 meters below seafloor (mbsf) where the

[1]Flood, R.D., Piper, D.J.W., Klaus, A., and Peterson, L.C. (Eds.), 1997. *Proc. ODP, Sci. Results*, 155: College Station, TX (Ocean Drilling Program).
[2]Lamont-Doherty Earth Observatory, Borehole Research Group, Palisades, NY 10964, U.S.A. PIRMEZ@LDEO.columbia.edu
[3]Earth Sciences Department, Memorial University of Newfoundland, St. John's, A1B 3X5, Canada.
[4]University of Hawaii-SOEST, Honolulu, HI 96822-2219, U.S.A.

Previous Chapter | Table of Contents | Next Chapter

APC recovered ~100% of the succession. Core recovery in deeper intervals, using the extended core barrel (XCB), fluctuated dramatically. Many deep intervals thought to be sand rich yielded no recovery at all for several tens of meters and an average recovery of ~25%.

In mud-dominated submarine fans, the nature and distribution of sandy deposits are critical to understanding the sedimentary dynamics of fan development, in particular the initiation, growth, and abandonment of channel-levee systems. Integration of core data and seismic data indicates that the sand-rich intervals are generally coincident with the so-called high-amplitude reflection packet (HARP) acoustic units identified at the base of overbank deposits (Flood et al., 1991; Pirmez and Flood, 1995). Based on the spatial distribution of the HARP acoustic facies (Flood et al., 1991) and acoustic stratal patterns (Pirmez and Flood, 1995; Pirmez, 1994), the HARP units have been inferred to represent the deposits of sediment gravity flows generated during the initial phases of channel bifurcation.

In this paper, sand-rich intervals drilled on the Amazon Fan are characterized using wireline logging data, including Formation MicroScanner (FMS) electric-resistivity images in conjunction with cores and seismic reflection profiles. Wireline logs were compared with the available cores to calibrate, in a semiquantitative fashion, the electrical facies observed in the logs to the lithofacies of fan sediments. With this calibration in hand, it was possible to combine the detailed core description columns produced by sedimentologists during Leg 155 with new descriptions of the unrecovered deposits extracted from the FMS images. The nearly complete lithologic logs produced in this way allow a characterization of the history of events and sedimentary processes associated with channel bifurcation and initiation of channel-levee systems and the overall development of channel systems on the Amazon Fan. Using the continuous bed-by-bed sections derived from the FMS images, we determined bed-thickness statistics for the sand-rich intervals to assess whether bed thickness follows power-law distributions as observed elsewhere, and whether such distributions vary with location on the fan. Finally, we briefly interpret our observations in the context of other modern and ancient submarine fans. The detailed characterization of the deposits of a particular environment in a modern fan, where the morphology and spatial characteristics are also well defined, is of particular interest to understanding turbidite sequences in ancient fans where, in general, knowledge of the morphology is severely limited by outcrop exposure.

BACKGROUND

The Amazon Fan is composed primarily of channel-levee systems that are grouped into larger units termed "levee complexes" (Damuth et al., 1988; Manley and Flood, 1988; Shipboard Scientific Party, 1995a) (Figs. 1, 2). Channel-levee systems on the Amazon Fan were supplied from the Amazon Canyon and consist of lens-shaped deposits of fine-grained overbank turbidites and coarser grained sediments at the channel axis. Channel-levee systems on the Amazon Fan reach total thicknesses of up to 500 m on the upper and middle portions of the fan and taper down to a few meters on the lower fan (Damuth et al., 1988). Laterally away from the channel axis, the overbank deposits of an individual channel can be traced with seismic reflection data for 10–20 km, but sediment carried by individual turbidity currents that spilled from the channel probably extends even farther, contributing to conformable "hemipelagic" deposits covering much of the fan; these can only be detected with cores and very high-resolution seismic techniques (Flood, Piper, Klaus, et al., 1995; Pirmez, 1994).

Damuth et al. (1983a, 1983b, 1988) and Manley and Flood (1988) showed that the distributary channel network on the surface and in the subsurface of the Amazon Fan developed as a result of repeated channel bifurcations. Because individual channel-levee systems onlap one another (Fig. 2), those authors suggested that bifurcation occurs by avulsion, and that only one primary pathway for turbidity currents is active at a time (see Pirmez and Flood, 1995; Pirmez, 1994, and Flood, Piper, Klaus, et al., 1995, for additional discussion and potential evidence for at least some simultaneous activity in multiple channels). During the development of a channel bifurcation, turbidity currents breach the levee of the channel and follow a path down the backside and along the interchannel topographic depression. The pathway above the bifurcation site continues to be used by subsequent turbidity currents, whereas a new channel segment eventually develops downslope of the bifurcation point. The segment of the parent channel below the bifurcation point becomes abandoned and subsequently buried by the overbank deposits of the new channel system.

The relative stratigraphy of the channel-levee systems has been worked out by Damuth et al. (1983b), Manley and Flood (1988), and Pirmez (1994). A detailed stratigraphy is available for the Upper Levee Complex of Manley and Flood (1988), including the channel-levees of the Orange-2 Channel to the Amazon Channel (Figs. 1A, 2). These channel-levees probably all formed within the last 50 k.y., according to the age assigned to the underlying mass-transport deposits (MTDs) by Piper et al. (Chapter 39, this volume). This chronology implies ultra-fast linear sedimentation rates exceeding 25 m/k.y. for individual channel-levee systems (Flood, Piper, Klaus, et al., 1995). The development of several channel-levee systems during a single glacial lowstand of sea level suggests that channel bifurcations are probably not directly related to major eustatic sea-level fluctuations (Flood, Piper, Klaus, et al., 1995; Pirmez and Flood, 1995).

The morphology and internal structure of the most recently active Amazon Channel are reported by Pirmez (1994) and Pirmez and Flood (1995). This channel displays a concave-up, relatively smooth longitudinal talweg depth profile, suggesting that the channel morphology resulted from an equilibrium with the turbidity currents that traveled through it during the last glacial lowstand of sea level. The smooth longitudinal profile is the result of spatial variations in talweg aggradation and downcutting as well as planform sinuosity. The channel can be subdivided into reaches according to whether the talweg sits below or above the surrounding fan surface. Both in the upper and lower reaches of the channel, the talweg sits below the adjacent fan surface. Along the middle section of the channel, defined here as the "middle fan," both the talweg and levee crests are perched above the adjacent fan surface.

If two points along the talweg are separated by a distance *a*, measured along the channel centerline, and a shorter straight-line distance *b*, then channel sinuosity is defined as *a/b*. The overall sinuosity of Amazon Channel is low. Along the middle section of the channel, however, the channel sinuosity is high, locally reaching a value of 3.

Channel bifurcation dramatically changes the morphology of the channel system, by imposing a shorter route to local base level (i.e., the interlevee topographic low). Because of the perched nature of the meandering channels and relatively steep levee backsides, an abrupt change in gradient, or *knickpoint*, is introduced on the talweg profile at the bifurcation site (Pirmez and Flood, 1995). Seismic reflection data indicate erosion of the underlying levee flank below the bifurcation sites along Amazon Channel and the development of onlapping reflections within the valley downslope (Pirmez, 1994; Pirmez and Flood, 1995). This onlapping unit is composed mainly of high-amplitude reflections (HARs), forming a HARP. Flood et al. (1991) inferred that this acoustic facies represents an interbedding of sand-rich deposits of unchannelized turbidity currents that descended the fan from sites of channel bifurcation, and turbidites formed at the mouths of channels. Pirmez and Flood (1995) show that the HARP unit has complex stratal patterns with evidence for local truncation, onlap, and small channels, suggesting the amalgamation of multiple units. Above the bifurcation sites, the resolution of the available seismic reflection data is not sufficient to determine whether downcutting of the pre-existing talweg occurred, because reflections beneath the channel axis tend to be obscured by side echoes (Pirmez and Flood, 1995; Flood, 1987). However, several other lines of evidence point to significant reshaping of the talweg profile after bifurcation: (1) total sed-

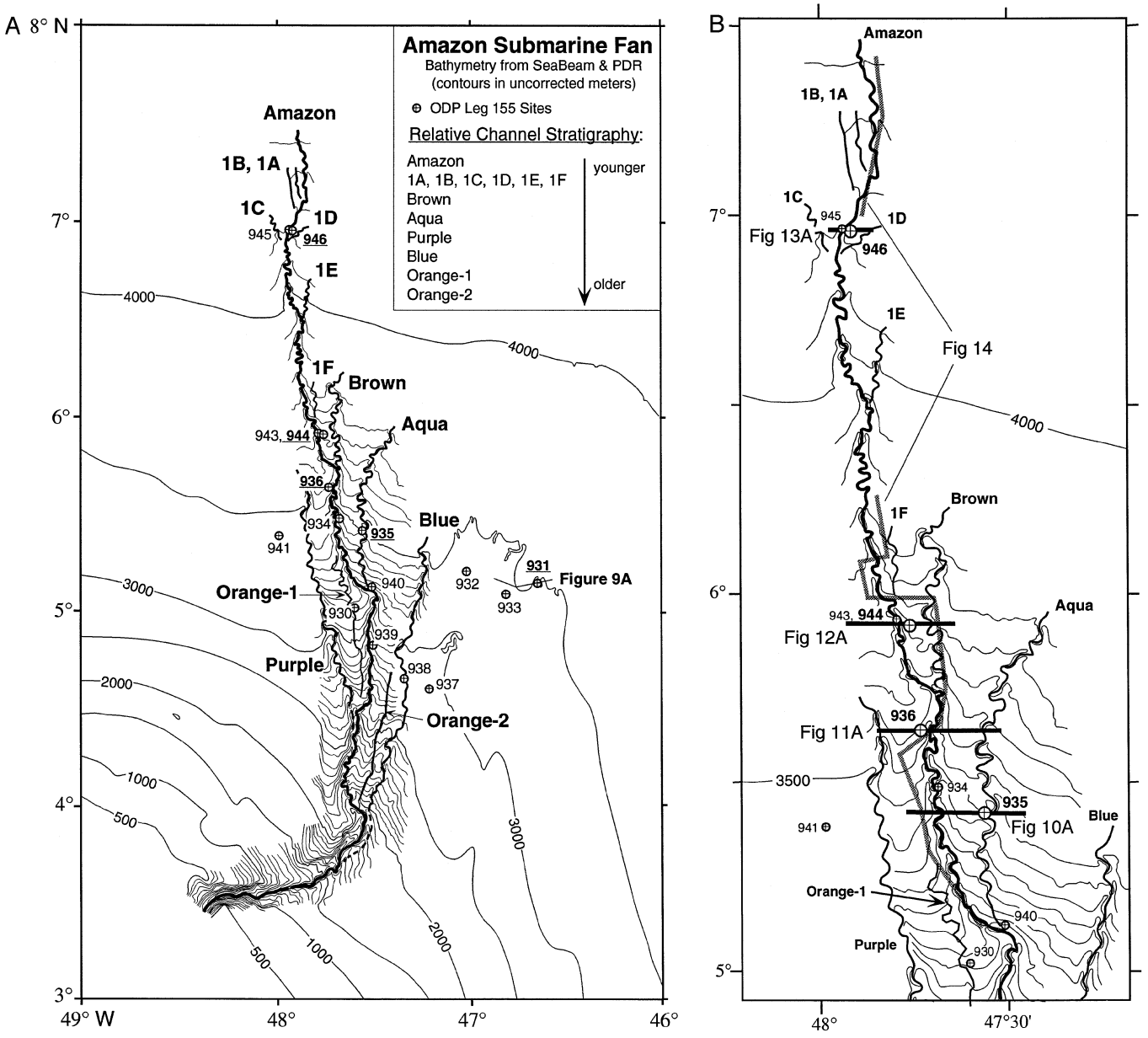

Figure 1. Location of sites on this study (931, 935, 936, 944, and 946). **A.** Amazon Fan channels, locations of Leg 155 sites, and location of a seismic line (Fig. 9A) across Channel-Levee System 5 at Site 931. **B.** SeaBeam bathymetry of Amazon Channel and locations of the seismic lines shown in subsequent figures (Figs. 10A, 11A, 12A, 13A, 14). Modified from Pirmez (1994) and Flood et al. (1991).

iment thickness is about the same both above each bifurcation (parent channel deposits) and below (new channel deposits), indicating that the talweg above was at least the site of marked sediment bypass if not erosion; (2) the channel above each bifurcation was the site of rapid changes in planform sinuosity, suggesting that other processes besides downcutting played a role in adjusting the longitudinal talweg profile; (3) the talweg of an abandoned channel on the upper middle fan (the Purple system; Fig. 1A) presently is at a depth shallower than the adjacent talweg of Amazon Channel, indicating active downcutting after bifurcation; and (4) the talweg of Amazon Channel on the lower fan, across one of the youngest bifurcations mapped (the 1C bifurcation; Fig. 1B), has a pronounced V-shape and cuts into the flank of the abandoned channel. These observations imply that erosion and reworking of the talweg and overbank deposits after bifurcation plays a significant role in the readjustment of the longitudinal talweg profile of the channel. Although downcutting and sinuosity reduction upslope lower the talweg profile, rapid accumulation in the valley downslope of the bifurcation raises the profile, eventually erasing the knickpoint introduced at the bifurcation site.

INTERPRETATION OF FMS IMAGES

In this paper, we examine in detail the wireline logging data from Sites 931, 935, 936, 944, and 946, with the objective of producing continuous bed-by-bed sections of the fan sediments in the sections of poor core recovery to complement the bed-by-bed sections derived from detailed core descriptions aboard ship (Shipboard Scientific Party, 1995b–i). The log-based bed-by-bed sections were derived primarily from the analysis of FMS resistivity images of the borehole wall, complemented by cores where available and other wireline logs (principally gamma-ray, resistivity, velocity, and density logs). The

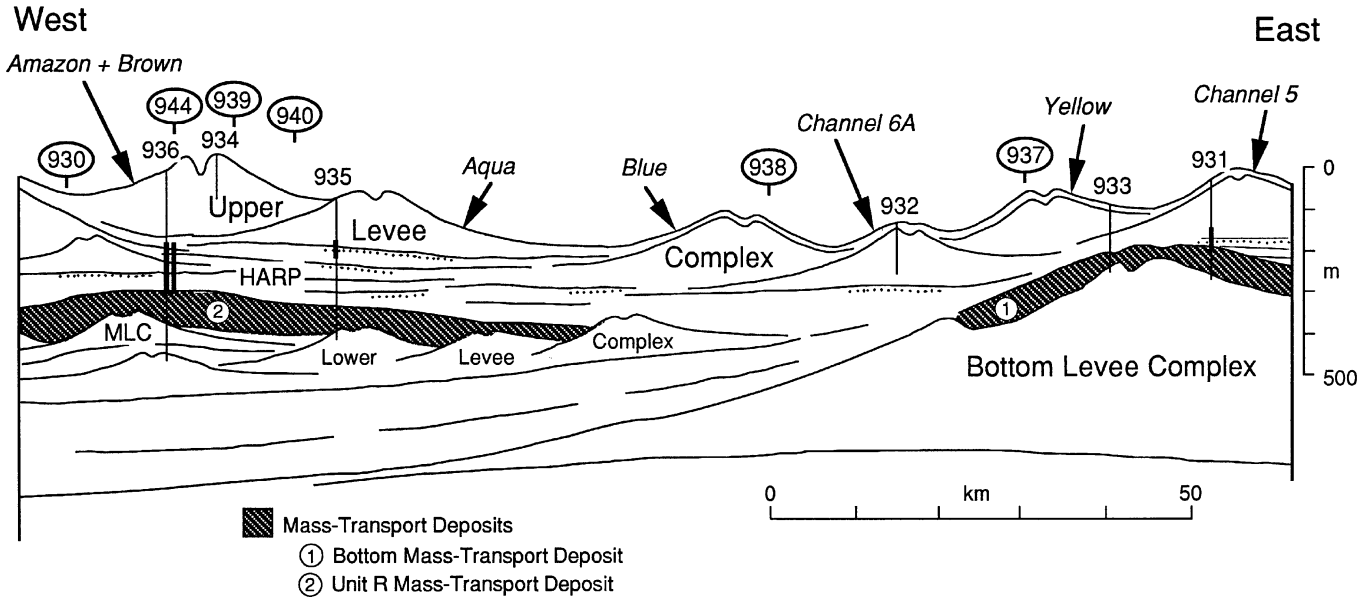

Figure 2. Schematic cross section of the upper Quaternary sediments of Amazon Fan at about the 3500 m bathymetric contour (based on Manley and Flood, 1988). Sites 936, 934, 935, 932, 933, and 931 are along this cross section; depths of penetration at these sites are shown (bold parts of each borehole = location of FMS-based sections in Fig. 3, back-pocket foldout). The other sites (circled site numbers) are projected into this cross section from farther upfan or downfan (Site 944), and are placed so as to accurately reflect the channel-levee system that was penetrated. Stacked channel-levee systems of the Upper Levee Complex are labelled. MLC = Middle Levee Complex. Site 946, discussed in this paper, is too far downfan to be projected into this cross section. Modified from Flood, Piper, Klaus, et al. (1995).

result is a well-constrained interpretation of the intervals of poor core recovery, particularly in the HARP intervals near the base of channel-levee systems. The essentially continuous bed-by-bed sections created by combining the FMS-based sections with core-based sections are then interpreted in the context of the seismic stratigraphic units identified on the fan.

Measurement Principles

The FMS is a four-pad microelectrical resistivity device that allows detailed investigation of vertical and lateral variations of formation resistivity (Serra, 1989). Formation resistivity is measured in 64 buttons: two rows of eight on each pad. Electrical current flows from the buttons into the formation and returns to the tool body. Current intensity variations in each button are proportional to the formation resistivity. The tool has a shallow depth of investigation. Data quality is very sensitive to poor pad contact with the borehole wall caused by borehole rugosity. The resistivity values obtained are relative, because the current flow is continuously adjusted during logging to optimize the tool operating range under varying bed resistivity. Resistivity measurements are recorded every 2.5 mm, and the vertical resolution of the tool is of the order of 2.5 cm, although beds thinner than 2.5 cm can be detected if the resistivity contrast is high (Serra, 1989). Data processing uses measurements recorded by a three-axis accelerometer placed in the tool body to correct the cable depth measurement for irregular tool motion in the hole. As a result, the button resistivity in different rows can be properly aligned. Fine tuning of the image is further provided by cross-correlating the resistivity measurements at adjacent buttons. Data from a three-axis magnetometer in the tool body allow the images to be oriented with respect to true north. The individual resistivity values are then binned into color or gray-scale classes to produce an image of the borehole wall that can be displayed at a computer workstation. In the gray-scale images reproduced here, darker shades mark lower resistivity values.

During FMS runs, all four pads rarely recorded good quality images at the same time. Poor image quality can result from a large borehole diameter, but images are often degraded even in borehole sections in gauge (~25 cm diameter). We attribute this to borehole rugosity at a scale of the order of the pad dimensions (~10 cm), borehole ovalization (which occurred often), and unconsolidated mud sticking to the pads. The latter is the source of vertical "streaks" observed in many images. Fortunately, two or more pads displayed good contact with the borehole in most cases, permitting the identification of bed boundaries and resistivity characteristics, but preventing the detailed interpretation of structures such as cross-lamination and the determination of paleocurrent directions.

In addition to the FMS data, gamma-ray, acoustic, density, and neutron porosity logs were particularly useful in identifying the sand-rich sections (detailed descriptions of tools and measurement principles can be found in Schlumberger, 1989). Sand-rich intervals displayed overall low gamma-ray, high sonic velocity, high density, and low neutron porosity values. The logs from the different runs were corrected for borehole diameter variations, shifted to meters below sea floor (mbsf) and correlated to each other, using the gamma-ray data from each individual run. The sonic and density logs were used to tie logging depths to travel time in the seismic reflection data using synthetic seismograms (Shipboard Scientific Party, 1995b–i). The vertical resolution of the geophysical logs is ~1 order of magnitude coarser than the FMS tool, but these lower resolution data were nevertheless quite useful to delineate the major contacts and to aid in the interpretation of the lithofacies from FMS images.

Image Interpretation

Formation resistivity depends primarily on the resistivity of the formation fluid, the connectivity of the pore space, and mineralogy. The high cation exchange capacity of clay minerals generally leads to lower formation resistivity in clay-rich beds. In the largely unconsolidated sediments encountered on the Amazon Fan, the pixel tone of the images tends to be correlated with grain size, so that silt and sand beds and laminae show lighter tones and muddy sediments show darker tones. Similar observations are reported by Serra (1989) and

Hiscott et al. (1992). Because the current flowing through each button is not calibrated to absolute resistivity, a quantitative calibration of image tone to sediment texture is difficult. As a result, the interpretation of bed boundaries and structures within beds is more firm than are assessments of the absolute grain size of individual layers.

The images were printed at a scale of 1:6 and interpreted side by side with both conventional well logs and the detailed bed-by-bed descriptions and photographs of cores produced aboard ship (Shipboard Scientific Party, 1995b–i). Bed boundaries were marked on the images and correlated to coring depths in an attempt to calibrate the images. In the thin-bedded silts and silty clays, a direct match between images and cores is practically impossible on a layer-by-layer basis, but the overall interval can be correlated. Direct matching of core and image was only possible where thicker beds or distinctive groups of beds and bed boundaries occurred. In these intervals, we were able to calibrate, in a qualitative manner, the image tone and character to the visual descriptions of grain size and facies in the cores.

In a number of cases, the identification of unique beds in intervals of essentially complete core recovery permitted a determination of the presence or absence of constant offsets between core depths and logging depths. Such discrepancies were noted in Holes 935A (~2 m) and 946A (~2–3 m). Potential sources of mismatch include errors in drill-pipe measurements, errors in logging depth due to cable stretch, and errors in log-log correlation and depth matching. In FMS data from two separate tool deployments in Hole 946A in the interval 92–126 mbsf, there are variable offsets up to more than 1 m in the apparent depths of unique features in the FMS images. These fluctuating log-log offsets are attributed to errors in the accelerometer-based correction of FMS images. Specifically, where the tool becomes temporarily stuck, the FMS processing software attempts to detect and correct for the stuck intervals, but there are often small errors in the automatic detection (Pratson et al., 1995).

The characteristics of the FMS images, including bed thickness, resistivity variations within beds (often associated with grain size grading), type of bed boundary (erosional, sharp, and gradational), and structures (lamination, presence of resistive or conductive clasts, and bioturbation) allow a classification of the HARP deposits into electrical facies. After comparing images to cores in all holes, the image characteristics could be confidently used to assign deposits to a lithofacies where cores were not available. Using the image tone together with gamma-ray logs, we then assigned an approximate grain size to each bed. The resulting interpretations are plotted as bed-by-bed sections using the same conventions employed in producing bed-by-bed sections from core descriptions (Flood, Piper, Klaus, et al., 1995). The log-derived sections (Fig. 3, back-pocket foldout) are plotted together with (1) the bed-by-bed sections based on cores in the same interval, (2) the total gamma-ray curve (SGR), and (3) acoustic velocity.

The convention of ODP is to assign the depth of a core to the top of the interval through which the drill bit advanced. This procedure is based on an assumption that partial recovery results from sediment being lost through the core catcher during core retrieval. Using FMS images from intervals of less than 100% core recovery, we were able in several cases to reposition cores below the top of the cored interval. In most cases, these partially recovered cores had to be placed either near the center or in the lower part of the interval drilled, suggesting that partial recovery resulted from sediment being washed out in front of the bit during coring.

Electrical Facies and Sedimentary Facies

Examples of FMS images and cores that typify the range of facies of the Amazon Fan are shown in Figures 4–8. We give a brief description of each facies encountered to illustrate how specific lithofacies appear on the images. We believe that all but perhaps one electrical facies observed on the images is represented in the cores. This suggests that although there are several intervals of poor core recovery, the log-derived bed-by-bed interpretations complement the core descriptions with a high degree of confidence.

Color Banded Muds

Intervals of thinly laminated silty clays with barely perceptible grain-size variations, but pronounced alternation of light and dark bands were common in Amazon Fan cores (Fig. 4B). The color bands were ephemeral, and the whole core would oxidize to a nearly uniform olive gray after a few hours of exposure to air. This color banding can be seen in close-up photographs taken soon after the cores were split (Fig. 4C). Subtle changes in resistivity are present in an FMS image of the same interval (Fig. 4A). In the core, the light and dark bands are ~2–6 mm and 1–3 mm thick, respectively. There are ~20 resistive layers each ~20–30 mm thick in the corresponding FMS image. A small contrast in resistivity presumably occurs between the color bands, but the FMS tool probably integrates the effect of several bands because they are thinner than the dimensions of individual buttons (6.7 mm). Small resistive spots in the image could be related to burrows, organic matter, or hydrotroilite “blebs” noted in the core. A clay-rich interval within a silt-laminated unit (Fig. 4D) shows interbedded intervals of thin laminations and intervals with a mottled appearance (pads 2 and 3), corresponding to bioturbated, mottled, and color-banded facies described in the equivalent Core 155-936A-13X (e.g., Fig. 5B).

Thin Laminae and Beds of Silt and Silty Clays

Thin-bedded and laminated silts and silty clays are common in overbank deposits of the channel-levee systems. In FMS images, this facies occurs as couplets of thin resistive layers 1–5 cm thick and conductive layers of variable thickness. The resistive lower part, which corresponds to silt, has a sharp base and commonly a quite sharp top as well (e.g., Fig. 5D, E, and FMS images and photograph from sediment penetrated by Core 155-936A-13X, shown in Fig. 5A–C). The tops of silt beds are commonly more gradational in those FMS images from thicker beds, suggesting that the tool cannot resolve grading in the very thin beds.

Thin to Medium Beds of Silt and Sand

This electrical facies is similar to the preceding facies, except that the resistive intervals are thicker (5–25 cm) and clearly display an overall upward decrease in resistivity suggestive of normal grading. The more conductive upper portion of these beds commonly displays faint parallel laminations. Examples of thin silt and silty-sand beds up to ~25 cm thick can be seen in Figures 4D (~112.1 mbsf) and 5C (~113.9 mbsf).

Medium to Thick Beds of Silt and Sand

This facies is characterized by beds 0.25–1 m thick with sharp, commonly erosional bases and normal grading. This facies forms a significant fraction of the HARP intervals drilled on Leg 155. Figure 6A displays two beds, 40–45 cm thick, with Bouma (1962) divisions T_a through T_c and perhaps T_d. Figure 6B illustrates silty-sand beds with T_b, T_c (cross-lamination), and T_d divisions.

Very Thick Sand Beds With or Without Clasts

With very few exceptions, all beds thicker than ~1 m recovered during Leg 155 contain mud clasts in variable concentrations (e.g., Fig. 7C, E). FMS images from several very thick sand beds display a pronounced lateral variability in resistivity, suggesting the presence of both conductive and resistive clasts varying from a few to several centimeters in diameter (Fig. 7A, B, D). In some cases, clasts contain evidence of internal laminations (e.g., Fig. 7A, pad 4 at 187.6 mbsf;

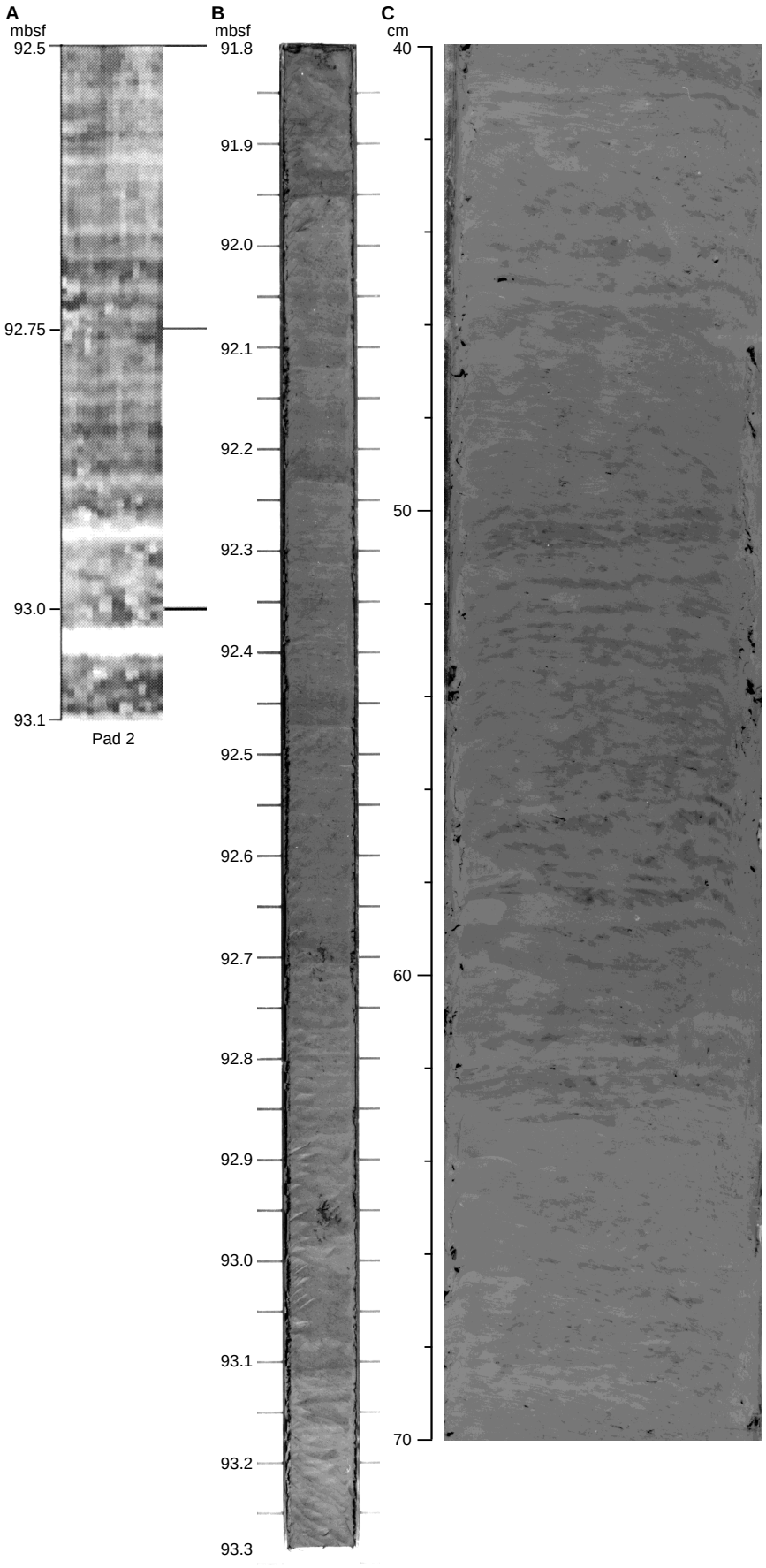

Figure 4. **A.** FMS image in Hole 931B, ~93 mbsf, within interval of color-banded muds (only pad 2 shown, image from FMS pass 2). **B.** Section 155-931B-11X-5, spanning 91.8–93.3 mbsf, showing faint color bands in otherwise homogeneous muds. Oxidation of core after splitting largely removed evidence of color banding. **C.** Close-up photograph of color-banded interval 155-931B-11X-2, 40–70 cm, taken soon after the core was split.

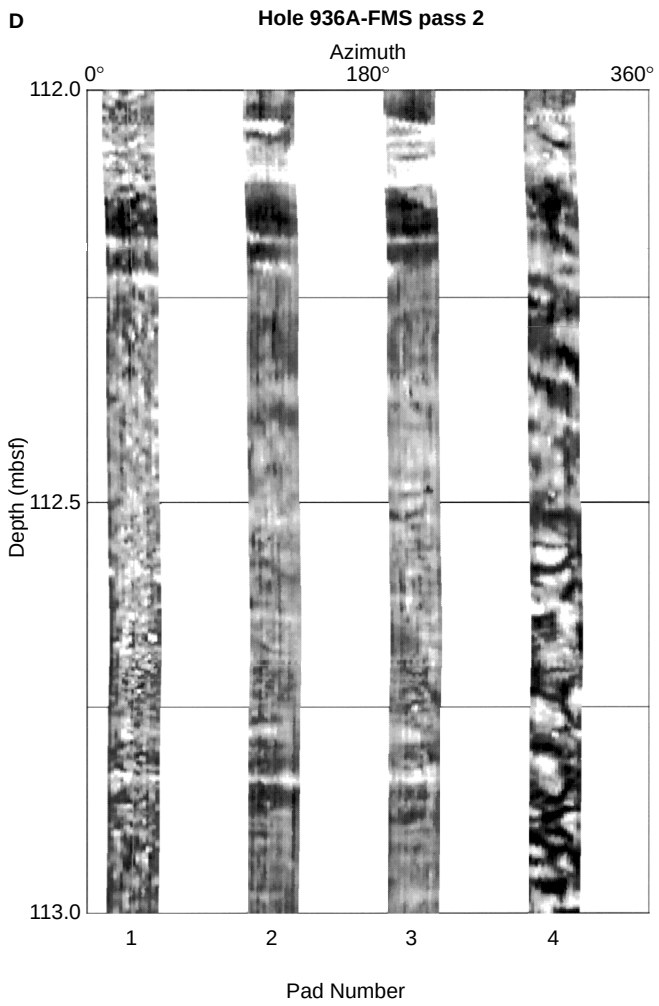

Figure 4 (continued). **D.** FMS image in Hole 936A, 112–113 mbsf, within interval of color-banded muds with rare silt laminae (image from pass 2).

Fig. 7B, pads 1 and 2 at 187.7 mbsf). Contorted beds, probably the result of folding of larger clasts or soft sediment deformation within the bed, were also observed within very thick sand beds (e.g., Fig. 7B, 187.4 mbsf). Where mud clasts are present in the cores, the gamma-ray log shows an increase in natural radioactivity. In the FMS-based bed-by-bed sections, the presence of clasts is only indicated where the image quality, together with a local increase in gamma-ray, warrant a definite interpretation. It is possible that more clasts are present than we were able to recognize.

Gravel and Scattered Clasts

One interval in Hole 946A (~240–260 mbsf) is formed of an electrical facies that does not appear to be represented in the cored material from Leg 155. Here, FMS images display an overall high resistivity and a number of rounded clasts with even higher resistivity floating in what is interpreted as a sandy matrix (Fig. 8). Gamma-ray measurements are low within this interval. The texture of this electrical facies resembles that of a pebble conglomerate described from the western Pacific by Hiscott et al. (1992). Elsewhere on the fan (Section 155-936A-36X-CC, 337.5 mbsf), hard-rock pebbles as large as 6 cm in intervals of very poor recovery suggest other gravel deposits (Shipboard Scientific Party, 1995d).

FMS images indicate that very thick sand-rich intervals are characterized by both clasts and irregular bedding (e.g., Fig. 5E, top), although in some cases poor hole conditions make it impossible to decide whether bed contacts are erosional. Many mud clasts retrieved in Leg 155 cores are more consolidated than in situ mud beds, suggesting that the clasts represent previously buried muds that were exhumed and incorporated into sand-rich sediment gravity flows. More consolidated clasts may appear as either resistive or conductive bodies in the images depending on the contrast with the matrix material. Resistive clasts are likely made up of partly compacted clays, although some carbonate-rich clasts were also observed in the cores. The presence of mud clasts in the thicker sand beds, and their general absence in beds thinner than ~1 m, is probably related to the erosive nature of larger flows.

RESULTS

In this section, we relate our logging results to seismic data. We then interpret the bed-by-bed sections derived from the logging data in relation to channel development, focusing on the intervals in which logging data augment the seismic interpretation of Flood, Piper, Klaus, et al. (1995). The sites are described in order of increasing water depth.

Site 931

Seismic Stratigraphy

Site 931 is located on the flank of Channel-levee System 5 on the eastern part of the middle fan (Figs. 1A, 2). The seismic reflection data (Fig. 9A) show that the channel system overlies a slump/debris-flow complex, the bottom mass-transport deposit (BMTD) of Piper et al. (Chapter 6, this volume). Two acoustic units can be discerned: (1) a lower unit, with HARPs that onlaps the BMTD and thins to the west; and (2) overlying overbank deposits, with overall low acoustic amplitude reflections, which downlap onto both the underlying HARP unit and the BMTD toward the west. Within the HARP unit, there is evidence for local truncation, probably associated with small channels that are not well resolved in the seismic reflection data.

Log Characteristics

Between 230 and 185 mbsf (Fig. 3, back-pocket foldout), logs show a variable response with several intervals indicative of sand beds (generally low gamma-ray, resistivity and neutron porosity, and high velocity and density). Thin sand beds and one very thick bed of sand with mud clasts were recovered near the base of this interval. The interval between 185 and 163 mbsf is marked by sharp upper and lower boundaries in the logs (Figs. 3, 9B). There is distinctly high gamma-ray and resistivity, and overall low density and velocity. Two cores within this unit (Cores 155-931B-19X and 21X) contain silt-laminated clays and silt beds (Fig. 3, back-pocket foldout). This high gamma-ray interval marks the top of reflections that dip gently and downlap toward the west, suggesting that during deposition of this interval, Site 931 was located west of the active channel or flow pathway. At ~163 mbsf, there is a sharp drop in gamma-ray values, followed by an overall upward increase in gamma-ray corresponding to the fining-upward sequence of Channel-levee System 5. The basal portion of Channel-levee System 5 between 163 and 137 mbsf shows several peaks of high velocity and has overall low gamma-ray activity, corresponding to the HARP interval associated with the base of this system. Above 137 mbsf, low-amplitude reflections that converge away from the channel axis correspond to the thin-bedded turbidites deposited on the levee of Channel-levee System 5.

Sedimentation Patterns from FMS Images

FMS data provide a complete characterization of the interval of incomplete recovery between 230 and 104 mbsf.

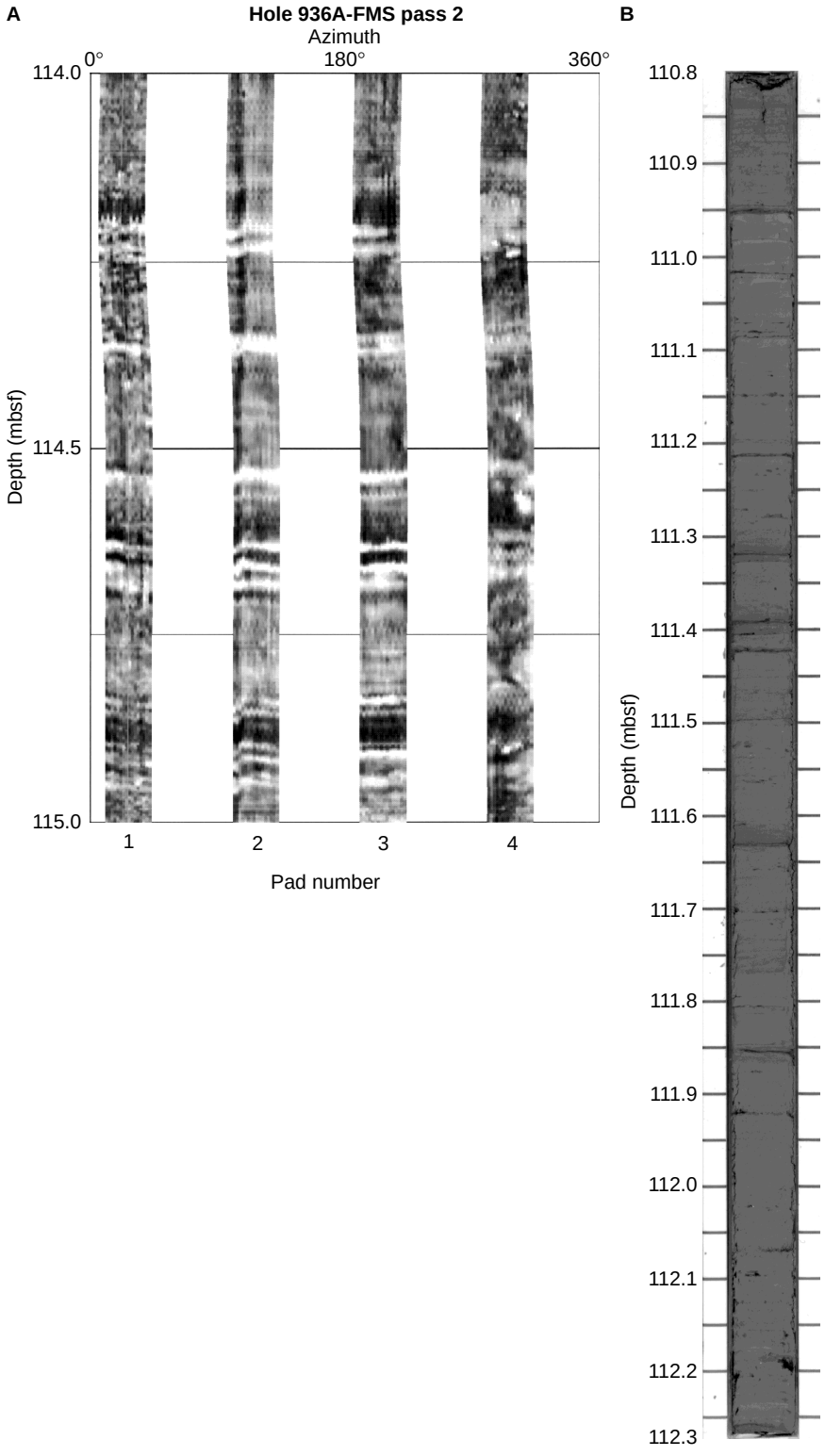

Figure 5. **A.** FMS image in Hole 936A, 114–115 mbsf, within interval of thin-bedded silty clays (FMS pass 2). **B.** Section 155-936A-13X-4, spanning 110.8–112.3 mbsf, which corresponds approximately to the depth interval imaged in **A**.

HARP Unit Between the Bottom Mass-Transport Deposit and Channel-Levee System 5

The interval between 230 and 163 mbsf cannot be placed within the stratigraphic framework of the fan because seismic coverage is poor in this area. The BMTD lies below 235 mbsf and is described elsewhere (Piper et al., Chapter 6, this volume). Above the BMTD, there is a series of four thick-bedded clusters or packets, separated from one another by intervals of thin-bedded silty clays, silts, and probably sands (Fig. 3, back-pocket foldout). The clusters contain four to ~15 beds ranging in thickness from 5 to 10 cm to 4.5 m. Some of the thicker beds apparently contain abundant mud clasts. Some clusters appear to be very sharp based (e.g., 178–175 mbsf, 204–196 mbsf; Fig. 3, back-pocket foldout), whereas others appear to show a gradual increase in bed thickness at the base (e.g., 193–185 mbsf). The top of this interval is characterized by thin-bedded silts and silty

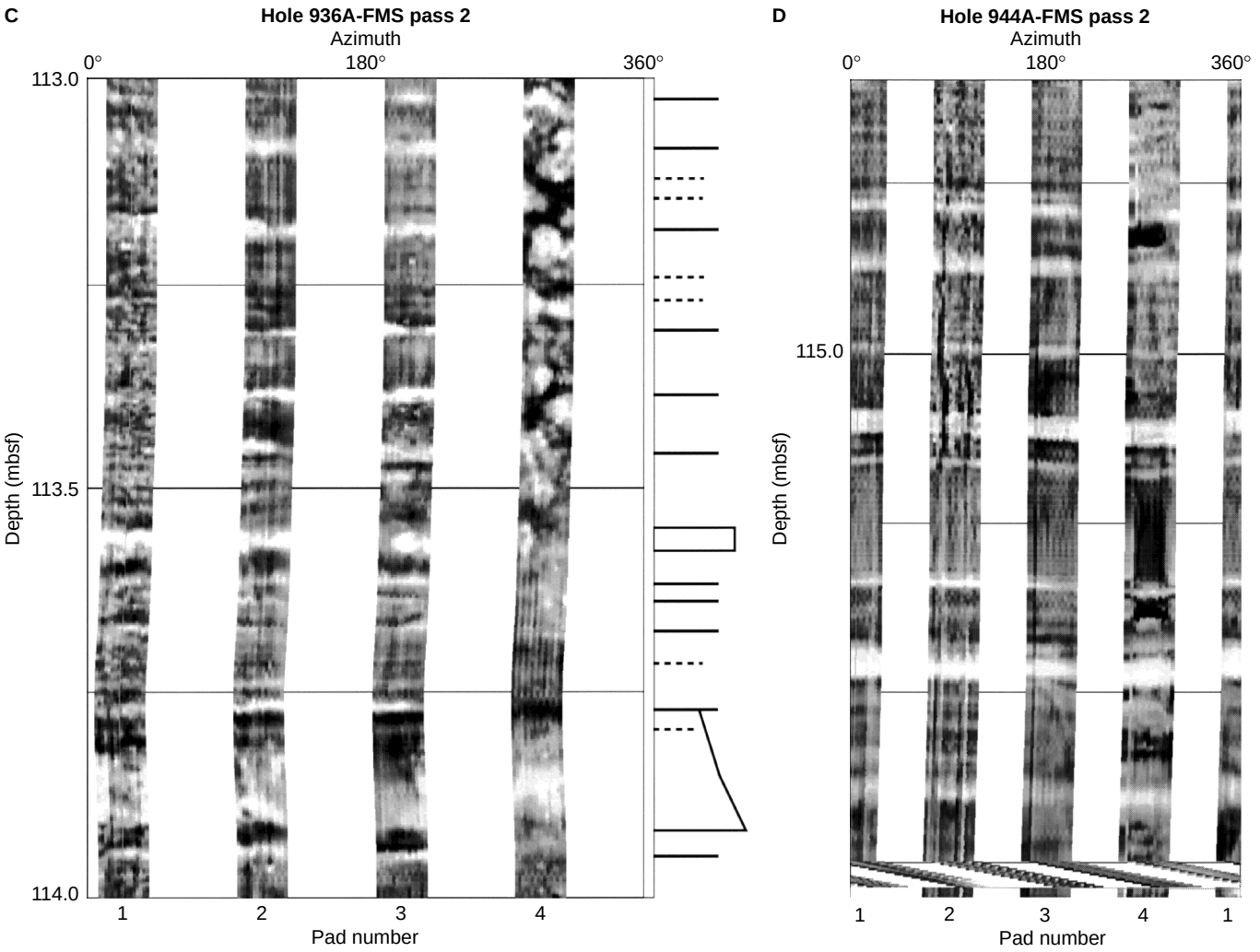

Figure 5 (continued). **C.** FMS image in Hole 936A, 113–114 mbsf, within interval of thin-bedded silty clays (FMS pass 2), showing a few thicker silty and silty sand beds (outlined on right) with evidence of grading. **D.** FMS image in Hole 944A, ~115 mbsf, within interval of thin-bedded silty clays and silty-sands (FMS pass 2).

clays. The succession between 185 and 163 mbsf resembles overbank deposits recovered elsewhere on Amazon Fan levees.

Channel-Levee System 5

The base of Channel-levee System 5 corresponds to an angular unconformity in the seismic data, correlated to 163 mbsf at the top of a muddy interval. Between 163 and 137 mbsf, many sand beds are thicker than 1 m; one bed exceeds 2 m. Sand beds appear structureless with graded tops and occur in clusters of less than ten beds, varying from thick to very thick beds interbedded with intervals containing thin beds and laminae, probably of silt and fine sand. This interval corresponds to the HARP facies observed in the seismic data, marking the onset of development of Channel-levee System 5 (Fig. 9A). This onset is characterized by the abrupt deposition of a 0.75-m-thick sand bed above thin-bedded silty clays, followed by an apparent upward increase in sand bed thickness from 163 to 155 mbsf. The top of the HARP unit in seismic data corresponds to 137 mbsf in the lithologic column. This depth marks the transition from thick and very thick (often >1 m) beds and bed packets below to overall thinner (all <1 m) beds of silt and silty sand above (Fig. 3).

Above 137 mbsf, the seismic data indicate the onset of overbank deposition from Channel-levee System 5. The interval between 137 and 110 mbsf mostly contains medium to thick beds of silt, which range in thickness from 0.1 to 1 m. Beds have sharp bases and graded tops. The characteristics of the thicker beds in this interval suggest the presence of fine sands and in some cases mud clasts (Fig. 3, back-pocket foldout). There is an apparently abrupt decrease in the frequency of silt-sand beds at 110 mbsf, corresponding with the top of an upward increasing trend in the gamma-ray log (Fig. 9B). Otherwise, the lower overbank deposits associated with Channel-levee System 5 appear to be composed of a random succession of silt-sand beds interbedded with more thinly laminated silty clays. A few intervals, ~2 m thick each, may represent thinning-upward cycles (e.g., 134–132 mbsf, 128–126 mbsf; Fig. 3, back-pocket foldout).

Site 935

Seismic Stratigraphy

Site 935 is located on the western flank of the abandoned segment of the Aqua Channel-levee System, ~100 km downslope of the Purple bifurcation site (which led to the initiation of the Aqua Channel) and 30 km downslope of the Aqua bifurcation site (which led to the abandonment of the Aqua Channel; Fig. 1B). Seismic interpretation shows that the upper part of the hole penetrated the overbank deposits of the Amazon and Aqua Channels (Fig. 10A). The Aqua Channel

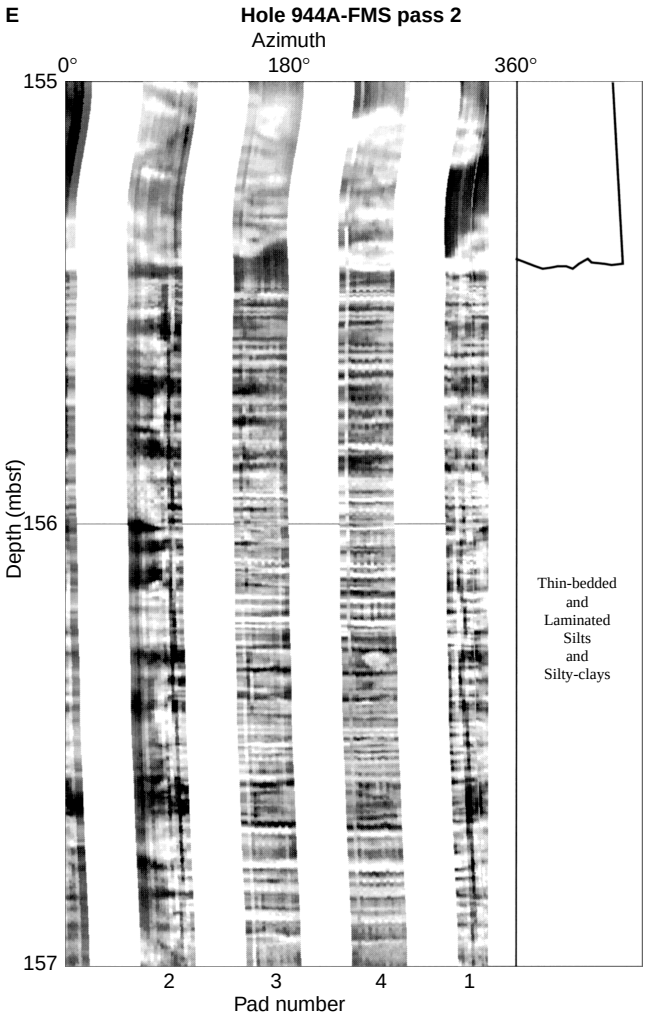

Figure 5 (continued). **E.** FMS image in Hole 944A, 155–157 mbsf, showing an interval of thin-bedded silty clays in erosional contact with a sand bed above (FMS pass 2).

overbank deposits show overall low-amplitude reflections that downlap to the west. A downlap surface within the Aqua levee apparently marks a bifurcation occurring farther downslope along the Aqua Channel (Pirmez, 1994). The base of the Aqua system is an angular unconformity onlapped by high-amplitude, subhorizontal reflections. This basal unconformity coincides with the top of the Orange-1 channel system at this site. The unconformity is locally eroded by small channels, including one apparently penetrated by the borehole. Toward the east, erosion appears to have been more extensive beneath the present axis of the Aqua channel system. Pirmez and Flood (1995) and Pirmez (1994) show that upslope of the site, the basal unconformity of the Aqua channel system is overlain by a mixture of acoustic facies, including subhorizontal HARPs and acoustically transparent units with internally hummocky or chaotic reflections. A series of HARs beneath the base of the Aqua system corresponds to the Orange-1 channel system. The latter overlies the Unit R MTD (Piper et al., Chapter 6, this volume).

Log Characteristics

Below 152 mbsf, the downward decreasing gamma-ray, low resistivity, low neutron porosity, and high bulk density suggest the presence of thick and very thick sand beds. Correlation with the seismic reflection data indicates that this interval corresponds with the Orange-1 stratigraphic unit. A muddy mass-flow unit with high gamma-ray response (152–118 mbsf; Fig. 10B) appears to be the oldest unit to onlap the top of the Orange-1 channel system. It subsequently pinches out toward the west. Correlation with seismic data away from Site 935 suggests that the Purple bifurcation unconformity (base Aqua system) is at the base of this muddy MTD. The HARs near the base of the Aqua system (Aqua HARP) correspond to a ~20-m-thick interval of sediments (118–100 mbsf, logging depths) with low gamma-ray and high acoustic velocity (Fig. 10A, B). This was an interval of poor recovery, but Core 155-935A-12H contains three thick massive beds of medium sand (Fig. 3, back-pocket foldout). West of the pinch-out of the mass-flow unit, these sands of the Aqua HARP directly overlie the Purple bifurcation unconformity.

Sedimentation Patterns from FMS Images

We focus our interpretation of the FMS images to the interval between 118 and 100 mbsf (logging depths), corresponding to the HARP unit at the base of the Aqua Channel-levee System. Deeper sands were poorly imaged by the FMS. The 118–100 mbsf interval is characterized by a cluster of beds, with thicknesses ranging from a few centimeters up to 4 m (Fig. 3, back-pocket foldout). Beds have sharp to erosional bases, and in at least one case contain a number of mud clasts. Subtle changes in image tone within thick resistive intervals and steps in the gamma-ray profile suggest bed amalgamation. There is no distinct trend in bed thickness within this interval. The entire 18 m of this HARP unit appears to be composed of a single cluster of sand beds, interbedded with thin silt and silty sand beds.

The top of the HARP unit at 99 mbsf (coring depth, equivalent to 100.5 mbsf logging depth) marks the onset of Aqua overbank deposition. There is an abrupt bed-thickness and grain-size decrease at this level. Above, thin and medium beds of silt are gradually replaced by thinner beds and increased clay content in an overall fining- and thinning-upward succession (Shipboard Scientific Party, 1995c).

Site 936

Seismic Stratigraphy

Site 936 is located on the western levee of Amazon Channel about 60 km downslope of the Aqua bifurcation (Fig. 1B). The overbank deposits of the Amazon Channel system at this site contain sediment deposited in the Brown and younger phases of channel development (Fig. 11A). An angular and locally erosional unconformity marks the base of the Amazon Channel system, with a HARP onlapping the unconformity. Low-amplitude overbank reflections lie above this HARP and downlap progressively toward the west. Within the overbank deposits, a smaller scale downlap surface (with onlap near the channel axis) separates the Brown phase of sedimentation below and younger phases of channel development above (Fig. 11A; Pirmez, 1994; Pirmez and Flood, 1995). The base of the HARP unit at this site corresponds to a pronounced surface where the top of the Orange-1 and Purple Channel systems merge. Just west of the site, two small unleveed channels can be detected within the HARP unit, whereas to the east the HARP unit appears to thin rapidly, possibly because of erosion near the axis of Amazon Channel (Fig. 11A). Below the unconformity, HARs that are discontinuous, with evidence for local truncation and onlap, correspond to deposits formed at the distal end of the Orange-1 channel system (Figs. 1B, 11A).

Log Characteristics

Gamma-ray data in the lower part of the Orange-1 HARP unit (154–118 mbsf, Fig. 11B) show an upward decreasing trend. Recovery within this ~35-m-thick interval corresponding to the Orange-1

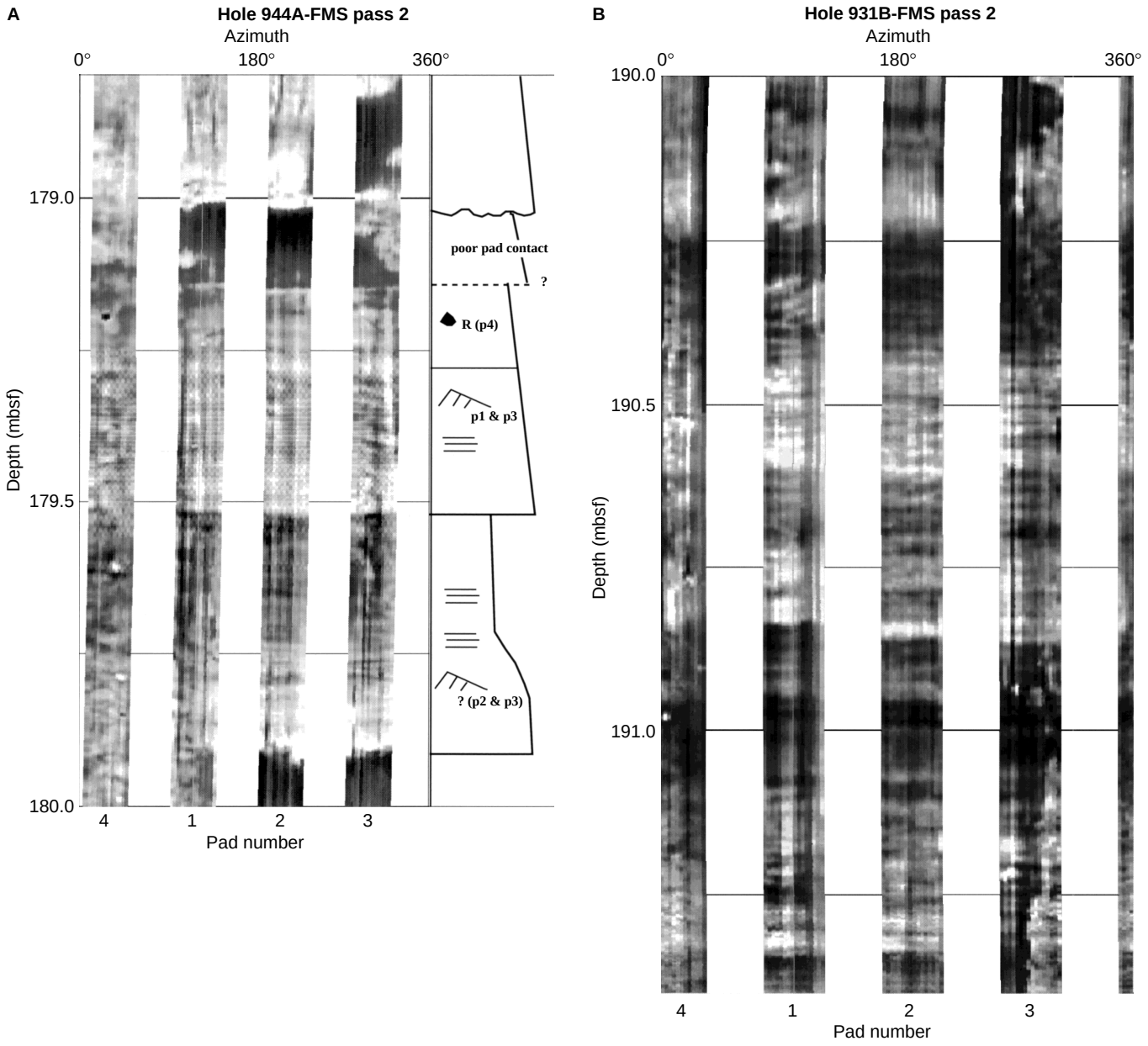

Figure 6. **A.** FMS image in Hole 944A, 179–180 mbsf, showing medium beds of silt and sand. Interpretation on right highlights sharp basal contacts and overall upward decrease in resistivity in each bed due to grain-size grading (FMS pass 2). **B.** FMS image in Hole 931B, 190–191 mbsf, showing medium beds of silt and sand (FMS pass 2).

system was very poor, except for thin-bedded, bioturbated silty clays just above the Unit R MTD. The muddy sediments of the Unit R MTD (294–154 mbsf; Shipboard Scientific Party, 1995d) are mostly characterized by high gamma-ray response (Piper et al., Chapter 6, this volume).

The Brown HARP unit corresponds to an decreasing-upward gamma-ray interval (99–79 mbsf) bounded above by thin-bedded silty clays and silty sands, and by silty clays below in the interval 118–99 mbsf (Figs. 3, 11B). The thin-bedded silty clays are commonly mottled with evidence for bioturbation, indicating an interval of lower sedimentation rates (Shipboard Scientific Party, 1995d). The bioturbated interval above (in Core 155-936A-8H) marks the top of a well-defined interval of upward increasing gamma-ray and upward decreasing velocity and resistivity (Fig. 11B), and this boundary at 99 mbsf is interpreted to correspond to the downlap surface between the Brown HARP and overbank deposits of the Brown levee. The bioturbated unit below the Brown HARP is difficult to assign to a particular phase of channel development because the top surfaces of three channel-levee systems merge at the site (Aqua, Purple, and Orange-1 systems; Fig. 11A). FMS data are not available between 82 and 72 mbsf. A large washout occurred between 76 and 79 mbsf, and the geophysical logs are unreliable in this interval.

Sedimentation Patterns from FMS Images

The bed-by-bed section derived from FMS images at Site 936 illuminates the interval of poor core recovery from the top of the Unit

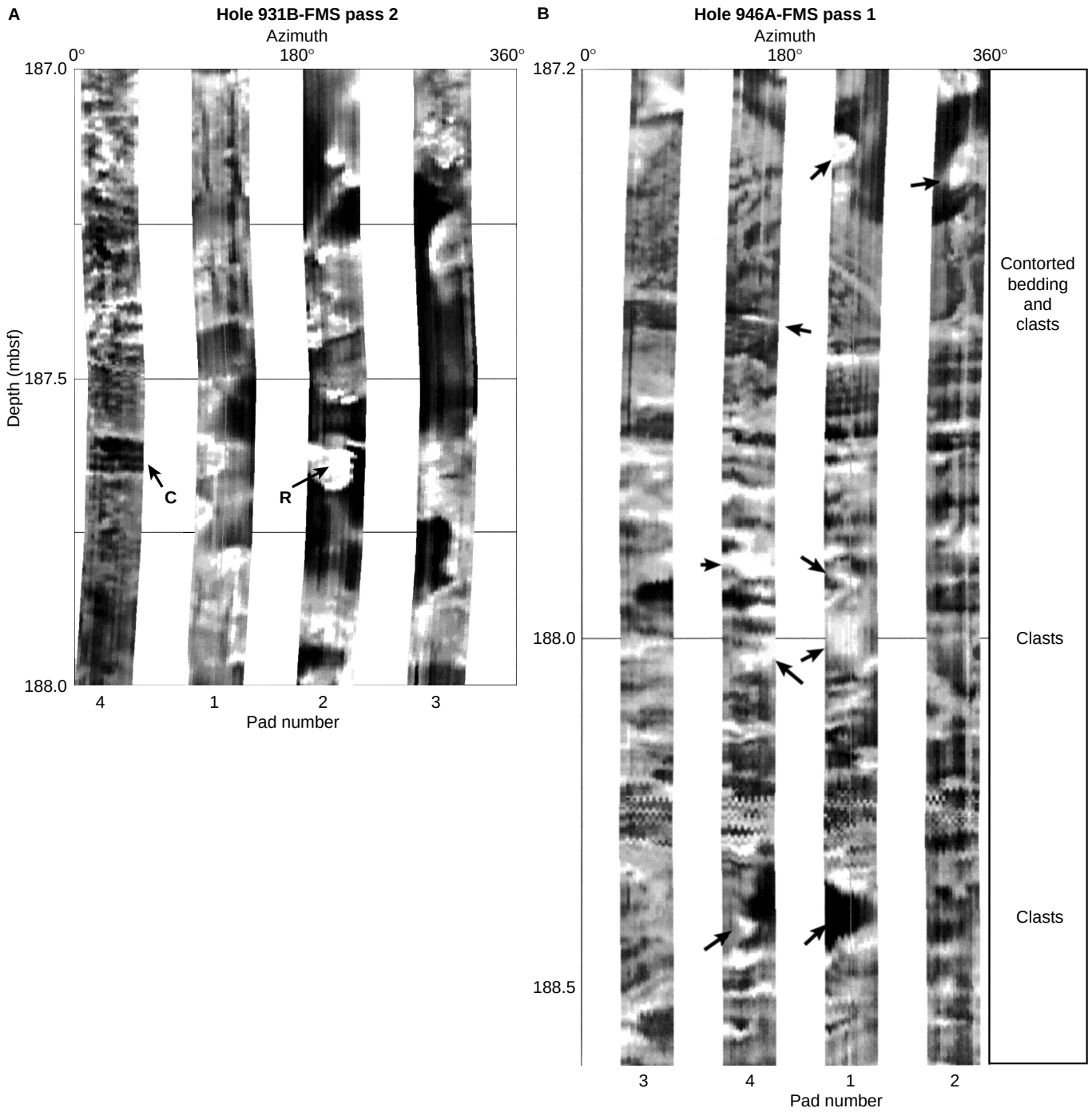

Figure 7. **A.** FMS image in Hole 931B, 187–188 mbsf, showing interval of thick sand beds with clasts (FMS pass 2). R = resistive clasts; C = conductive clasts. The darker areas in the pads 2 and 3 probably reflect poor pad contact with the hole. **B.** FMS image in Hole 946A, 187.2–188.5 mbsf, showing interval within a thick sand bed with clasts (arrows) and contorted bedding (FMS pass 1). **C.** Section 155-946A-21X-1, spanning 188.2–189.7 mbsf, from approximately the same interval seen in B. **D.** FMS image in Hole 946A, 205–207 mbsf, showing abundant dark (conductive) clasts, interpreted to be composed of mud, in a sand-rich matrix (lighter tones). There are apparently some resistive clasts above 206 mbsf but image quality is not as good as in the lower section (FMS pass 1). **E.** Sections 155-946A-23X-2 and 3, spanning 209.0–212.0 mbsf, interpreted to correspond closely to the interval imaged in D (based on offset between cores and logs, Fig. 3E, back-pocket foldout).

R MTD to the HARP unit at the base of the Brown Channel system (Fig. 3, back-pocket foldout).

Orange-1, Distal Purple, and Aqua Phases of Channel Development (154–100 mbsf)

The contact between the Unit R MTD and the Orange-1 system above is not well defined in the images, but medium beds of silt and sand (?) occur a few meters above the Unit R MTD in a thin-bedded unit between 154 and 147 mbsf. From 147 to 118 mbsf, several clusters of sand beds are present. These are characterized by low gamma-ray, and peaks of high velocity in the geophysical logs (Figs. 3, 11B). These clusters are interbedded with thin beds of silt and sand. The sand beds in the clusters range in thickness from a few centimeters up to 3 m, have sharp to erosional bases, and range from massive, to graded throughout, to graded only at bed tops. Many sand beds ap-

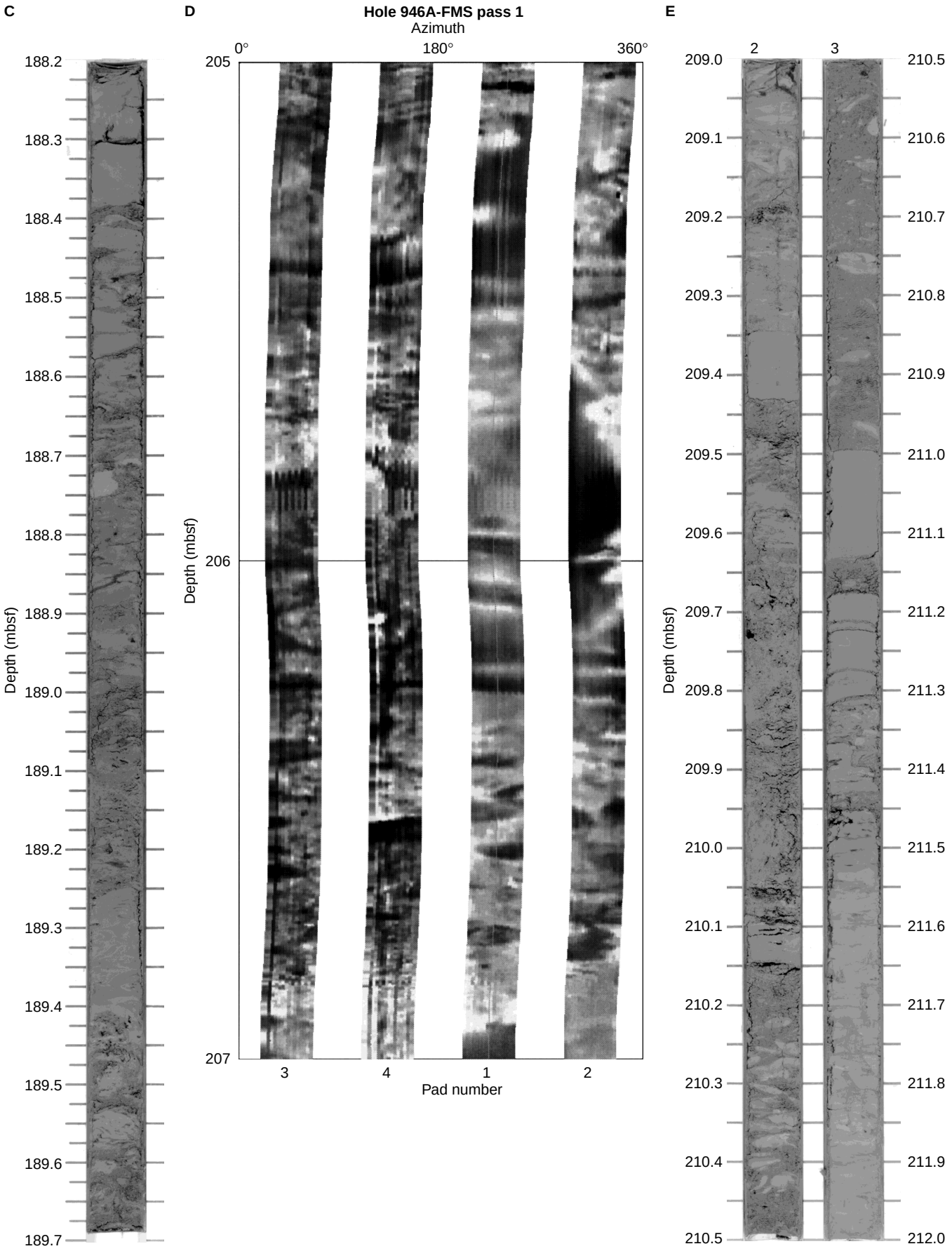

Figure 7 (continued).

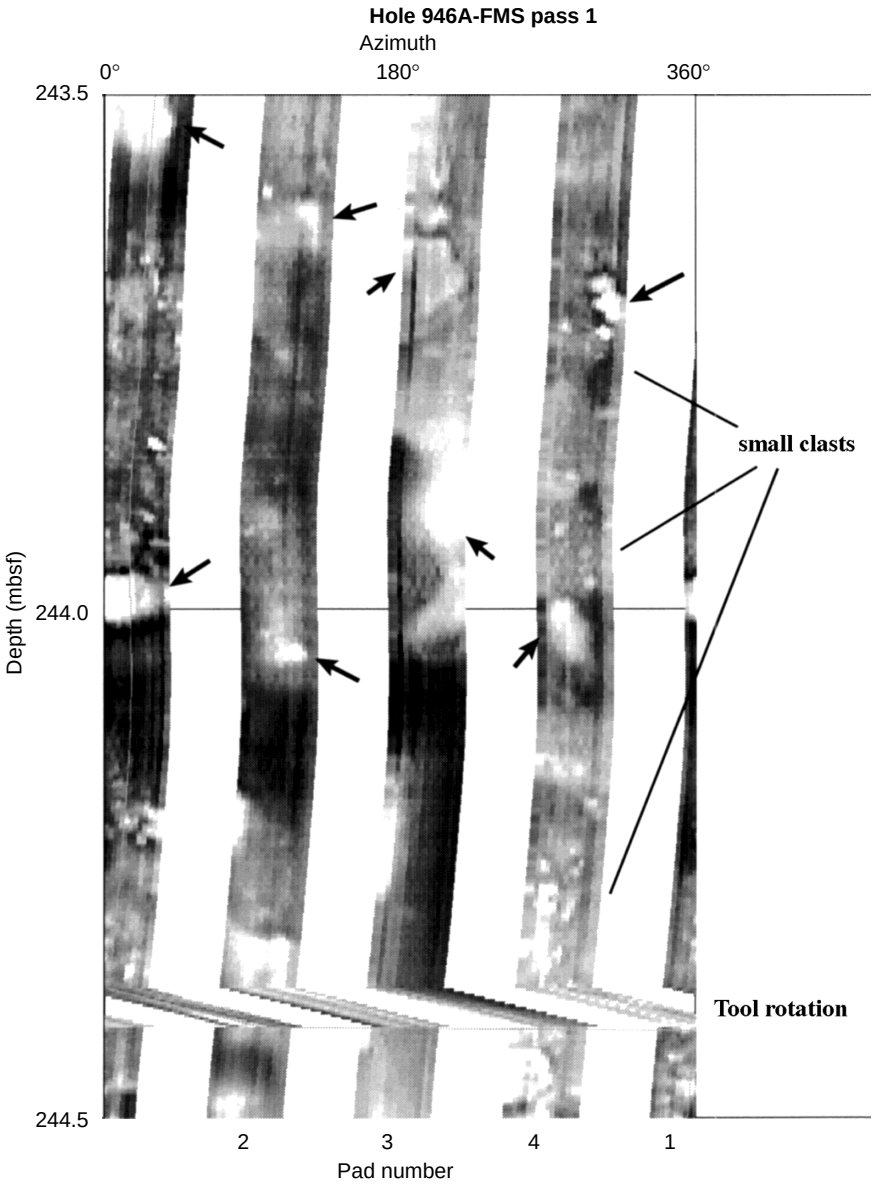

Figure 8. FMS image in Hole 946A, 243.5–244.5 mbsf, showing portion of a bed interpreted as a pebbly gravel (FMS pass 1). The very resistive clasts (arrows) may consist of lithified sediment similar to siltstone pebbles recovered elsewhere on the fan.

pear to have muddy tops. Some beds are amalgamated. Mud clasts are present in the thicker sand beds.

Overall, the sandy interval from 147 to 118 mbsf does not appear to have well-defined asymmetric trends. Each bed cluster includes only a few thick beds. The clusters, which are 4–6 m thick, have either very sharply defined bases marked by an abrupt increase in bed thickness (e.g., 146–142 mbsf) or more gradual basal contacts marked by an upward increase of bed thickness over a few meter interval (e.g., 140–135 mbsf, 131–118 mbsf). The sand bed clusters also tend to display sharp tops with an abrupt decrease in bed thickness and probably grain size as well (from sand to predominantly silty turbidites). The interval near the top of this unit, between 118 and 100 mbsf, is marked by an overall thinning-upward and fining-upward trend, from 10- to 25-cm-thick beds of silt/silty-sand at the base, to silt-laminated clays and thicker mud intervals toward the top.

Brown Phase of Channel Development

The unconformity beneath the Brown system marks the abandonment of the Aqua Channel and onset of medium to very thick sand beds at 99 mbsf (Fig. 3, back-pocket foldout). Sand beds in this interval range in thickness from 5 cm to ~2 m. Image quality is not particularly good here, and interpretation is based on less than four pads over most of the interval. The thicker beds appear more massive, although image tone suggests grading, particularly toward bed tops. Mud clasts in this interval were recognized in at least two beds that are ~2 m thick, although image quality prevents a detailed assessment of clast distribution. Thicker beds recovered in Cores 155-936A-10H and 11X contain abundant mud clasts, and in Core 155-936A-12X, a single, lithified siltstone pebble was recovered (probably displaced to the bottom of the cored interval by drilling disturbance). Sand beds are in most cases interbedded with low resistivity intervals interpreted as muds. The basal part of this unit shows a somewhat gradual increase in bed thickness over an interval of ~2 m (100–98 mbsf).

The top of the sand-rich Brown HARP was not imaged with the FMS, but other logs suggest an overall fining-upward trend from ~80 to 70 mbsf (Fig. 11B). The HARP is overlain by bioturbated silty clays at ~72 mbsf in Core 155-936A-8H (Shipboard Scientific Party, 1995d).

Site 944

Seismic Stratigraphy

Site 944 is located on the eastern levee of the Amazon Channel, ~12 km downslope of the Brown bifurcation (Fig. 1B). The overbank deposits penetrated in this levee were spilled from the channel sys-

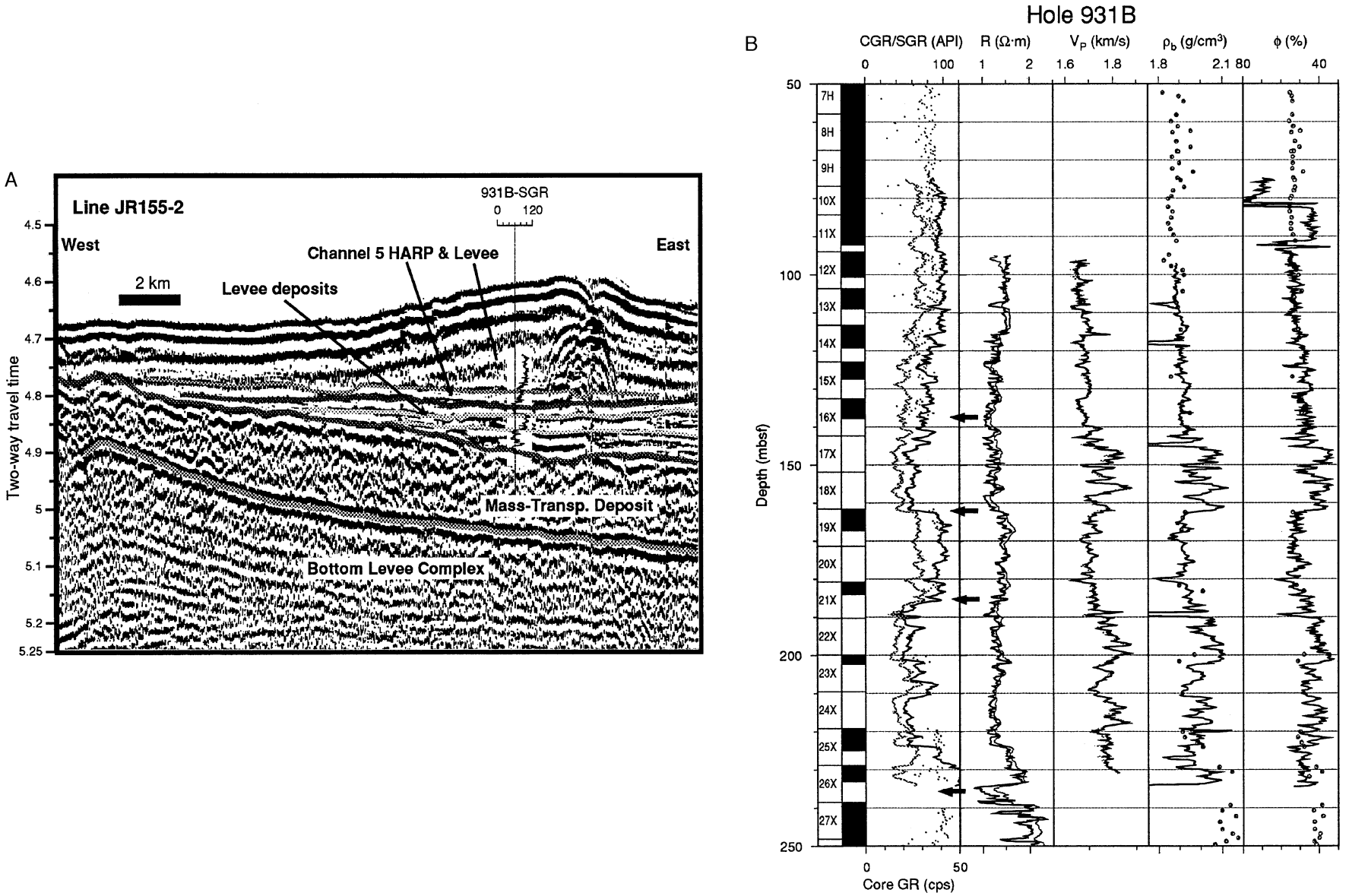

Figure 9. **A.** Interpreted seismic line across Site 931 (portion of *JOIDES Resolution* single-channel water-gun line 2, location in Fig. 1A; Flood, Piper, Klaus, et al., 1995). Integration of gamma-ray trace with seismic is based on a synthetic seismogram match, and traveltime is derived from a sonic log. **B.** Summary of geophysical wireline logs, physical properties measured on cores (dots), and core recovery (black) for Hole 931B. Bold arrows correspond to genetic unit boundaries explained in the text and on Figure 3 (back-pocket foldout).

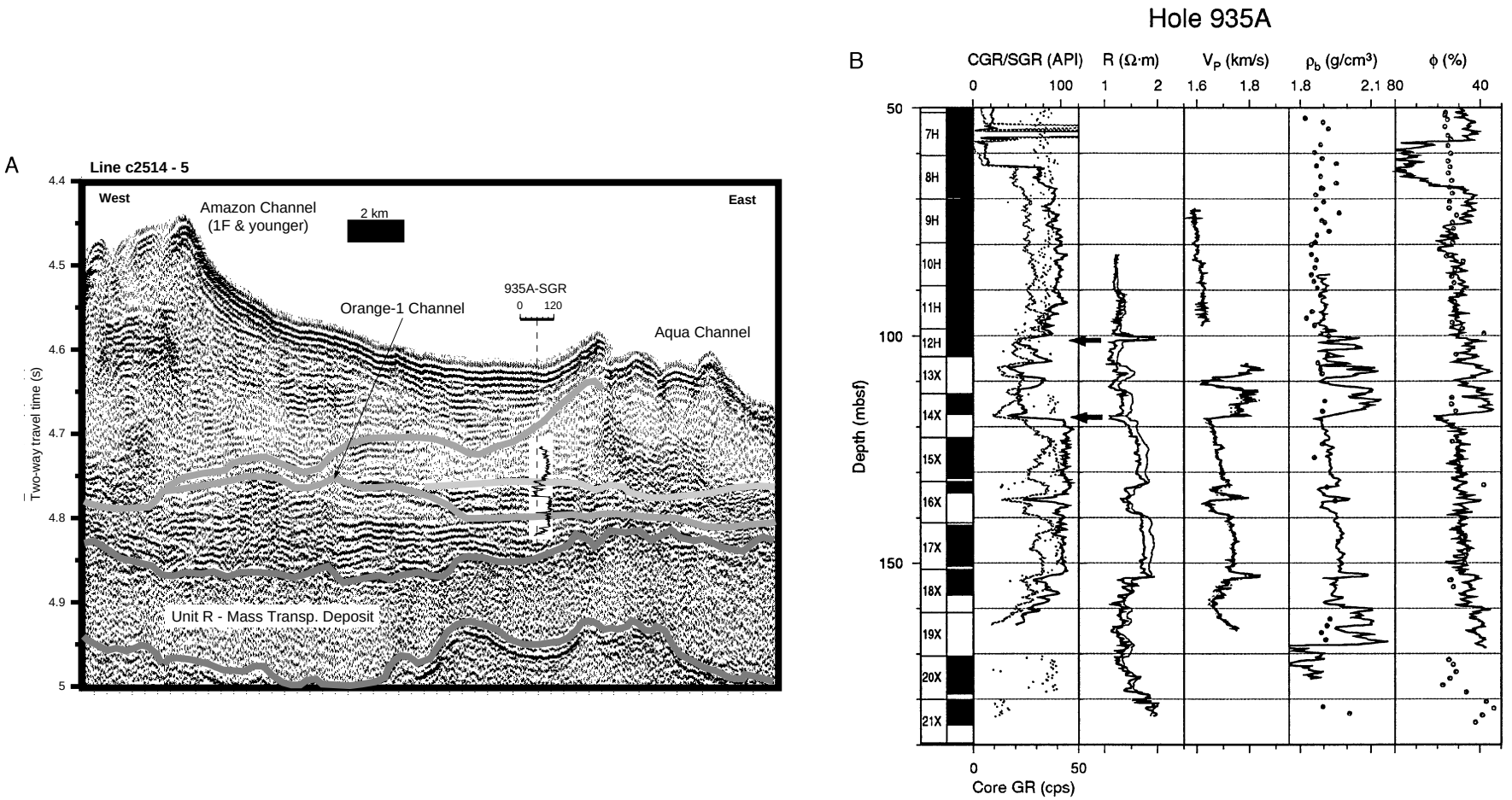

Figure 10. **A.** Interpreted seismic line across Site 935 (C25-14 single-channel water-gun line 5; location in Fig. 1B). **B.** Summary of geophysical wireline logs, physical properties measured on cores (dots), and core recovery for Hole 935A. Bold arrows correspond to genetic unit boundaries explained in the text and on Figure 3 (back-pocket foldout).

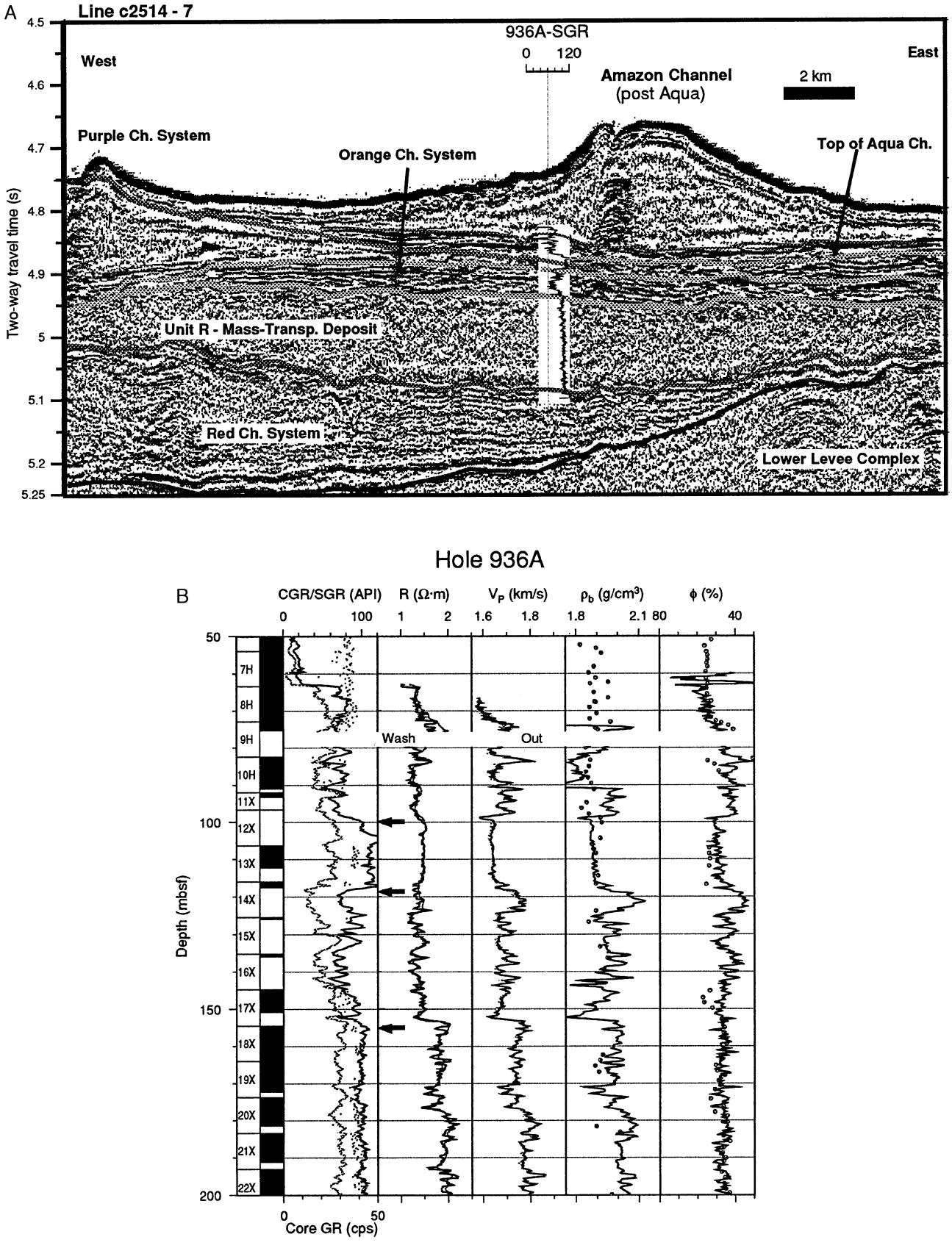

Figure 11. **A.** Interpreted seismic line across Site 936 (C25-14 single-channel water-gun line 7; location in Fig. 1B). **B.** Summary of geophysical wireline logs, physical properties measured on cores (dots), and core recovery for Hole 936A. Bold arrows correspond to genetic unit boundaries explained in the text and on Figure 3 (back-pocket foldout).

tems younger than Brown (i.e., 1F to Amazon; Pirmez and Flood, 1995). The switch from the Brown Channel to the Amazon Channel (1F phase of channel development) is marked by an angular unconformity on seismic profiles. Downlapping reflections above the unconformity correspond to the overbank deposits of Amazon Channel (Fig. 12A). Little erosion apparently occurred across the unconformity at the site; more significant erosion is observed to the west on the unconformity surface. The reflection marking this Brown bifurcation unconformity is apparently caused by an increase in the thickness and frequency of silt and silty sand beds seen in Core 155-944A-10H, corresponding to a short interval of lower gamma-ray response (Fig. 12A, B). A subtle coarsening and thickening trend is seen near the top of the Brown system (83–76 mbsf; Fig. 12B), suggesting that the seismic top of the Brown system overlies a thin succession that slightly postdates channel switching.

Log Characteristics

Between 192 and 140 mbsf, a series of HARs corresponds to deposits formed during the Purple and Orange-1 phases of channel development. The top of the Orange-1 sandy deposits is a sharp reflection that ties to an abrupt step in several logs at ~160 mbsf (Fig. 12B). From this point downward, low gamma-ray and peaks of high sonic velocity characterize Orange-1 deposits down to the contact with the Unit R MTD at 192 mbsf. Between 150 and 140 mbsf, the gamma-ray response shows a distinct upward decrease. This interval shows small channels and bi-directional downlap in the seismic data (Fig. 12A). The high gamma-ray interval between 140 and 130 mbsf, partly recovered in Core 155-944A-16X (Fig. 3, back-pocket foldout), may correlate in time with the Aqua or Purple phases of channel development, but the seismic data suggest that Aqua overbank deposits, if present, are thin.

In the logs, the base of the Brown Channel-levee System is a 6-m-thick interval of very low gamma-ray and high velocity between 130 and 124 mbsf (Fig. 12A, B). The seismic reflection corresponding to this sand interval can be traced to the east, beneath the Brown overbank deposits, and into the base of a thick unit of subhorizontal high-amplitude reflections (Brown HARP; Fig. 12A).

Sedimentation Patterns from FMS Images

Core recovery in sediments corresponding to the Brown, Purple, and Orange-1 phases of channel development was very poor (Cores 155-944A-14X to 21X; Fig. 12B). Fortunately, FMS data in the interval 190–125 mbsf enable a continuous lithologic section to be constructed (Fig. 3, back-pocket foldout).

Orange-1 Phase of Fan Growth

The interval between 189 and 160 mbsf is characterized by numerous sand beds ranging in thickness from 10 cm to 2 m. Geophysical logs and FMS images suggest mainly fine and medium sand, perhaps locally coarser. Fine sand was the coarsest material recovered in this interval (<1 m total recovery). Sediment just above the Unit R MTD (Core 155-944A-21X) consists of thin beds of silt and fine sand, but the FMS images are of poor quality at the contact. Thinning-upward cycles, each ~3–7 m thick, appear to occur between 183 and 167 mbsf (Fig. 3, back-pocket foldout). Between 167 and 161 mbsf, bed thickness gradually increases upward. Beds then abruptly become thinner (and probably siltier) above 160 mbsf. The reflection marking the top of the Orange-1 system falls in the interval of thin-bedded turbidites between 160 and 155 mbsf.

Purple and Aqua(?) Phases of Fan Growth

The interval between 155 and 130 mbsf corresponds to a small unleveed channel in the seismic data. It is characterized by two clusters of medium beds of sand. The sand beds range in thickness from ~5 cm to 1 m, although the few beds in the lower cluster are thicker (up to 1 m), whereas most beds in the upper cluster (146–141 mbsf) are thinner than 30 cm. The upper cluster, together with the thin-bedded interval below the cluster to a depth of 152 mbsf, shows a gradual upward increase in bed thickness over a ~10-m interval from 152 to 141 mbsf. The top of this asymmetric cycle is sharply overlain by very thin beds and laminae of silt and silty clay.

The interval marked by high gamma-ray between 140 and 130 mbsf appears to be characterized both in FMS images and Core 155-944A-16X by two intervals of mud with rare thin beds and laminae, separated by an interval containing more abundant silt laminae and thin beds (137.5–135 mbsf). We interpret the two muddy, bioturbated intervals in the core as the tops of the Purple and Aqua units. Such an interpretation is consistent with the available seismic reflection data, which cannot resolve the thin overbank deposits associated with the distal fringes of channel-levee systems.

Brown Phase of Channel Development

The low gamma-ray interval from 130 to 125 mbsf, which is tied in the seismic data to the basal unconformity of the Brown Channel-levee System, corresponds to a cluster of sand beds. The sand beds are 5 cm to 2 m thick. The thicker beds show evidence of amalgamation in the FMS images. This bed cluster has sharp basal and upper boundaries, with thin-bedded (silt) turbidites above and below (Fig. 3, back-pocket foldout). If our interpretations and correlation are correct, this cluster of beds is time-equivalent to the cluster of beds found between 100 and ~80 mbsf at Site 936. The overall thinning of this HARP unit downfan (from ~20 m to 10 m) is not surprising, given the ~33 km distance between the sites, and the slightly off-axis location of Site 944 (with respect to the thicker HARP interval beneath the Brown Channel; Fig. 12A).

Site 946

Seismic Stratigraphy

Site 946 is located on the lower Amazon Fan, ~6.5 km downslope of the 1C bifurcation (Fig. 1B; Pirmez and Flood, 1995). A series of discontinuous HARs is seen on the seismic profile across the site (Fig. 13A). The recognition of deposits of individual channels is difficult because seismic data coverage is sparse and because overbank deposits, with their characteristic acoustically transparent signature, are much thinner than in the middle fan, obscuring the acoustic contrast between different stratigraphic units.

A composite dip seismic section shows the downfan amalgamation of HAR units (Fig. 14, back-pocket foldout). Tracing of the reflections bounding the channel-levee systems on the middle fan to outer-fan Site 946 is uncertain. The available seismic data suggest that the borehole penetrated the lower fan equivalents of the Upper Levee Complex channels, the distal equivalents of the Red and Green Channel systems of the Middle Levee Complex and the Lower Levee Complex, and the top of the Bottom Levee Complex at Site 946 (Fig. 2). Specifically, the interval between the two highstand calcareous clays retrieved in Hole 946A is interpreted to correspond to the Green and Red systems (logging depths of intervals containing calcareous clays are 146–126 mbsf and 215–212.5 mbsf).

Log Characteristics

The logging data, in particular the spectral gamma-ray measurements, show signatures similar to those at Site 944 (compare Figs. 13B and 12B). The petrophysical characteristics of the sediments, based on neutron porosity, sonic, and gamma-ray logs in the interval between 212.5 and 146 mbsf, show two distinct units with characteristics similar to those of the Red and the Green systems, respectively, at Site 944 (Pirmez, unpubl. data; Flood, Pirmez, and Yin, this vol-

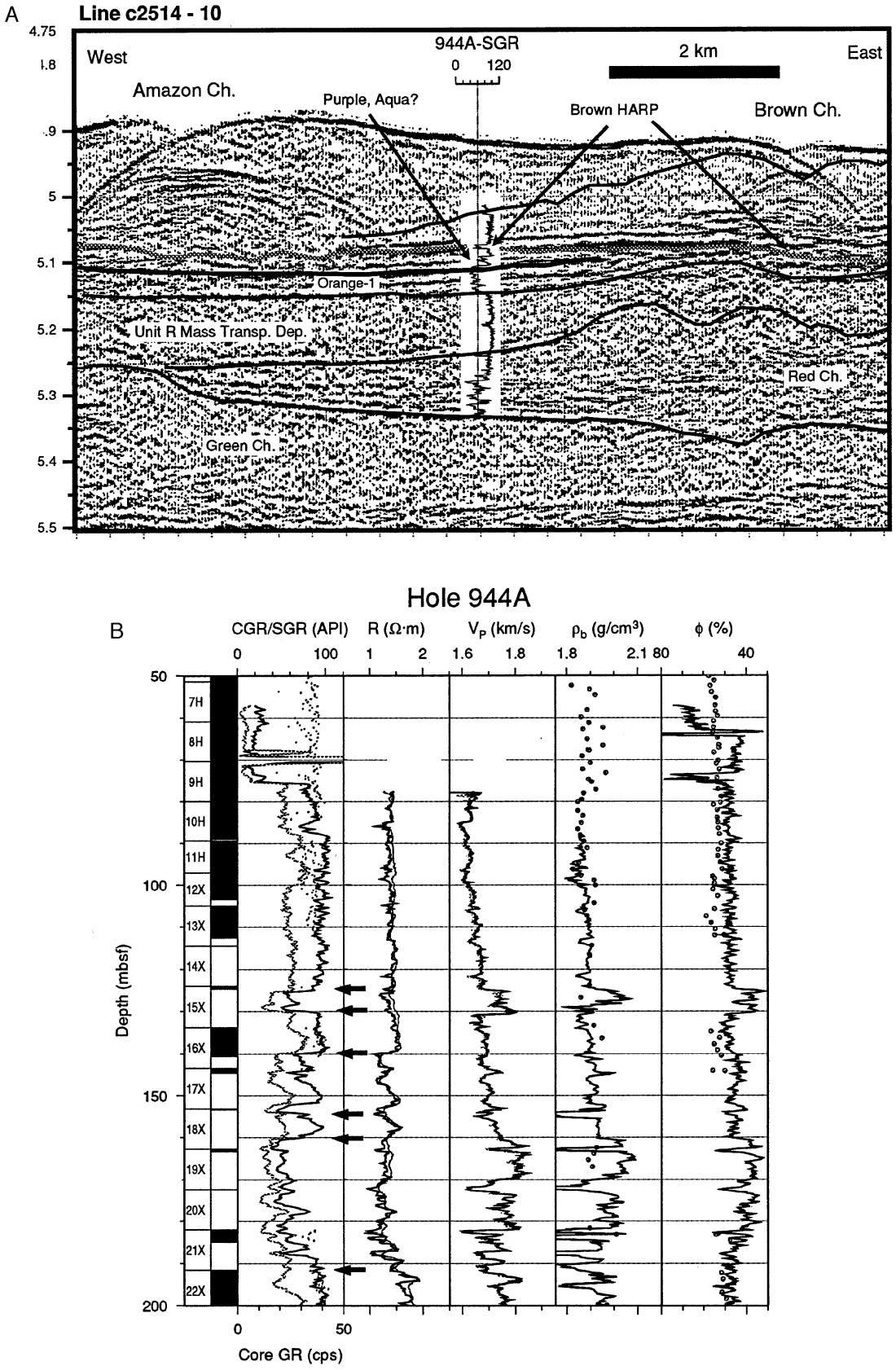

Figure 12. **A.** Interpreted seismic line across Site 944 (C25-14 single-channel water-gun line 10; location in Fig. 1B). **B.** Summary of geophysical wireline logs, physical properties measured on cores (dots), and core recovery for Hole 944A. Bold arrows correspond to genetic unit boundaries explained in the text and on Figure 3 (back-pocket foldout).

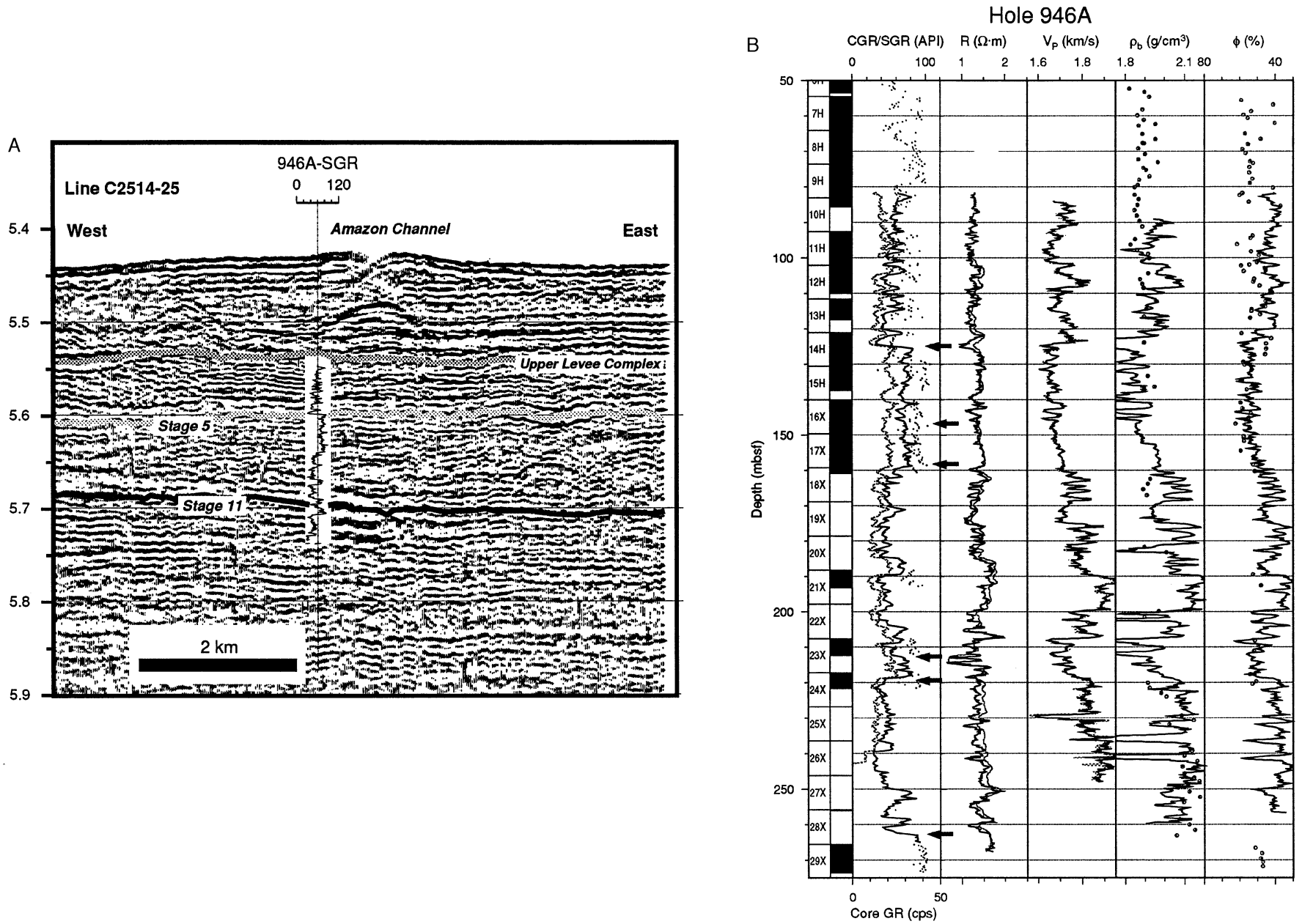

Figure 13. **A.** Seismic line showing location of Site 946 (C25-14 single-channel water-gun; location in Fig. 1B). **B.** Summary of geophysical wireline logs, physical properties measured on cores (dots), and core recovery for Hole 946A. Bold arrows correspond to genetic unit boundaries explained in the text and on Figure 3 (back-pocket foldout).

ume). This correlation suggests that the Red Channel-levee System is overlain by high-stand clays deposited during oxygen isotope Stage 5 (Maslin and Mikkelsen, this volume). The muddy Unit R MTD on the middle fan either pinches out upslope of Site 946 or is equivalent to one of the units above 146 mbsf. We discard this latter possibility because there are no muddy deposits at Site 946, 146–126 mbsf, similar to the Unit R MTD at Sites 935, 936, and 944.

Both below 159 mbsf and above 126 mbsf (logging depths), variable but generally low gamma-ray values indicate sand units 10–50 m thick. Some intervals with higher gamma-ray readings are sands heavily freighted with mud clasts (Fig. 3). The interval 130–90 mbsf has both good core recovery and a full complement of logs, permitting a detailed calibration of electrical facies to sedimentary facies.

Sedimentation Patterns from FMS Images

Core recovery within the upper 100 m or so was quite good. Here, we focus our analysis on the deeper interval, between 262 and 92 mbsf (logging depths, offset ~3 m from core depths; Fig. 3, back-pocket foldout). In this depth interval, core recovery was poor, and FMS data are essential to complete a lithologic interpretation. Our tentative seismic correlation places (1) the Upper Levee Complex (Orange-1 to Amazon phases of fan growth) above a set of highstand carbonate clays and associated muds that occur between 146 and 126 mbsf (logging depths), (2) the Red and Green systems between 146 mbsf and the top of a deeper set of highstand carbonate clays at 215–212.5 mbsf (logging depths), and (3) the Bottom Levee Complex HARP (older than oxygen isotope Stage 11; Shipboard Scientific Party, 1995a) between the deeper highstand carbonate clays at 215 mbsf and thin-bedded silts and muds below 262 mbsf. The fairly high quality of the FMS images at this site permits a detailed description of the succession.

Bottom Levee Complex

The base of Hole 946A in the Bottom Levee Complex is marked by thin beds and laminae of silt (Core 155-946A-29X). The base of the hole lies just above a pronounced regional reflection that can be widely traced higher on the fan. This reflection may correspond to a highstand interval like other widespread seismic reflections on the fan. The interval between 263 and 215 mbsf (logging depths) consists primarily of low gamma-ray sands with local increases associated with mud clasts seen in the FMS images. Coarse-grained beds are very thick. One bed, interpreted as a pebbly gravel (Fig. 8), is apparently 12 m thick (251–239 mbsf, logging depths). Groups of beds in the central part of the unit amalgamate to form a sand body ~32 m thick, with practically no intervening low-resistivity beds in the FMS images. Clasts are common in these thick beds and usually correspond to an increased gamma-ray response. This unit shows changes in bed thickness from slightly thinner at the base, reaching maximum thickness, and then decreasing toward 219 mbsf (logging depth). Rapid upward thinning is observed between 220 and 215 mbsf with 0.5–1 m sand beds below 219 mbsf overlain by thin (<5 cm) beds of silt and fine sand, and silty clay laminae. This thin-bedded interval is interpreted as overbank deposits.

Middle and Lower Levee Complexes

The interval between 212.5 and 146 mbsf can be separated into at least three major units with distinct bedding patterns (Fig. 3, back-pocket foldout). Between ~212.5 and 181 mbsf (logging depths), the thicker sand beds range in thickness from 1.5 to 9 m. This interval can be interpreted to contain two clusters of thick and very thick beds (212.5–200 mbsf and 195–181 mbsf), each with fairly sharp base and top, separated by an interval of thin-bedded turbidites. Abundant mud clasts are observed, and near the top of the interval clasts occur both at the base and top of what is probably a composite bed.

Between 181 and 159 mbsf (logging depths), beds are generally 0.1–1.2 m thick, with a maximum bed thickness of 2.5 m. No bed-thickness trends are evident in this interval, but the thicker beds appear to cluster both at the base and top of the interval.

Above 159 mbsf, there is an abrupt shift to thin beds and laminae of silt, characteristic of overbank deposits recovered elsewhere on the fan. The carbonate content increases upward, reaching maximum values between 146 and 130 mbsf (logging depths).

Upper Levee Complex

Above 126 mbsf (logging depth), there is good agreement between core- and log-based interpretations. However, there are differences between the resistivity images and the core descriptions that cannot be reconciled simply by linear adjustments of depth scales of the cores or logs. We believe that discrepancies between log- and core-based descriptions are probably caused by a combination of small errors in the nonlinear depth shifts applied to the logs and to coring-induced disturbance in the thick sand beds.

The Upper Levee Complex sediments have an abrupt basal contact at 126 mbsf, with thick and very thick sand beds overlying bioturbated muds below. Two groups of sand beds appear in the interval between 126 and 90 mbsf. The lower group (126–115 mbsf) contains beds ranging in thickness from 0.5 to 3 m, and the upper group (111–92 mbsf) has beds from 0.5 to 10 m thick. In each group, sand bed thickness appears to decrease upward.

Bed-Thickness Statistics

The depths of sand and silt bed boundaries in the continuous FMS-based bed-by-bed columns (excluding the column for Hole 935A) were digitized, allowing bed thicknesses to be sorted in ascending order. The data were then plotted in log-log space as the number of beds exceeding a particular thickness, N(thickness > T), vs. that thickness, T. Measured bed thicknesses range from 1 to 2 cm (the thinnest silt-sand beds that could be recognized in FMS images) to 18 m in HARP intervals (Fig. 15).

In other studies, it has been observed that the bed thicknesses of turbidites are distributed as a power law; that is,

$$N(\text{thickness} > T) \propto T^{-B};\ B > 0 \qquad (1)$$

where B is a measure of scaling in the turbidite sequence and may provide insight into the seabed morphology and transport processes (Hiscott et al., 1992; Rothman et al., 1994a, 1994b).

For single holes (Fig. 15A–E) or group of holes (Fig. 15F), the distributions of bed thicknesses in HARPs of the Amazon Fan show distinct "kinks" separating bed-thickness intervals in which N(thickness > T) appears to follow a power law (i.e., a straight-line segment in log-log space). The irregularity of curves for single holes (e.g., Fig. 15B) may reflect the relatively small number of beds in certain classes.

The scaling exponents for T < 0.3 m are about the same in all holes, ranging from 0.3 to 0.5, except for a small number of very thin beds (T < 0.08 m) at Hole 944A that show two distinct kinks in the distribution. For T > 0.3 m, the value of B is quite variable, with the distributions for Holes 936A, 944A, and 946A displaying two or more "kinks." The distribution at Hole 936A shows the largest B values (Fig. 15B), but this bed-thickness distribution is complex, rather than being formed of straight-line segments that might be interpreted as indicators of power-law behavior.

All beds thicker than 1 cm were combined into a single plot (Fig. 15F) in which there is a clear kink at a a bed thickness of ~0.35 m,

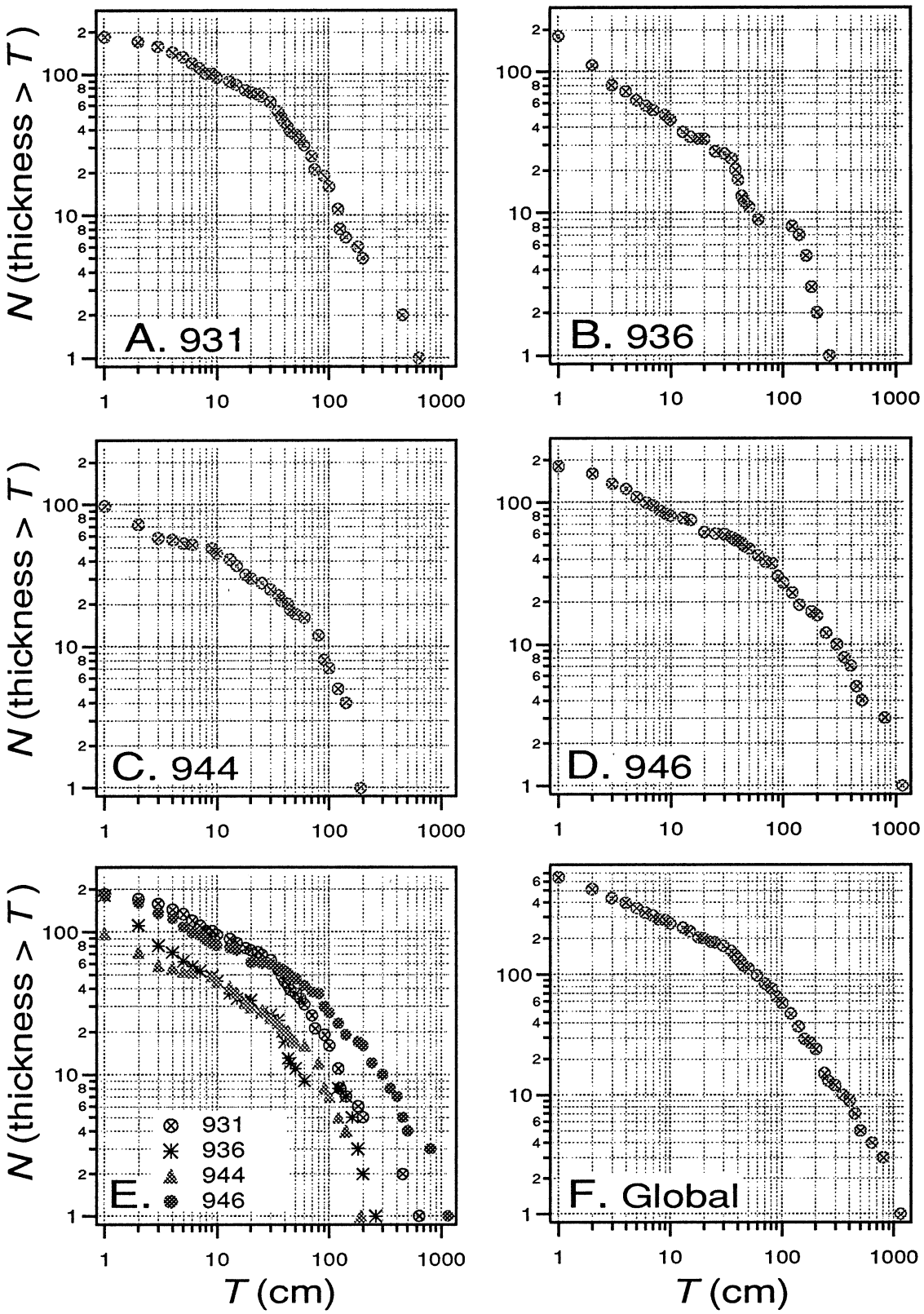

Figure 15. Log-log plots of bed thickness, *T*, vs. number of beds with thickness greater than *T* [*N*(thickness > *T*) vs. *T*]. Bed thicknesses were measured from the FMS images over the stratigraphic thickness displayed in Figure 3, back-pocket foldout. All beds thicker than 1 cm are included. **A.** Hole 931B (interval 23–98.9 mbsf; number of beds = 185). **B.** Hole 936A (interval 154.4–81.8 mbsf; number of beds = 180). **C.** Hole 944A (interval 188.5–124 mbsf; number of beds = 97). **D.** Hole 946A (interval 262.2–92.7 mbsf; number of beds = 180). **E.** All holes plotted together. **F.** All beds combined into a global data set (number of beds = 642).

separating two straight-line (i.e., power-law) segments. For $T < 0.35$ m, $B = 0.4$, whereas for $T > 0.35$ m, $B = 1.3$. For comparison, Hiscott et al. (1992) found $B = 1.1$ for some Izu-Bonin volcaniclastic turbidites, and Rothman et al. (1994a) found $B = 1.4$ for the Kingston Peak turbidite section.

DISCUSSION

Sand-Rich Units and Amazon Fan Sedimentation Processes

Thick bedded to very thick bedded intervals of sand, 5–25 m thick, characterize HARPs that onlap an angular-erosional unconformity at the base of several channel-levee systems, including Channel-levee System 5, and the Aqua, Brown, and Amazon (1F) Channel-levee Systems. In each of these HARP units, the sand deposits are commonly bounded by thin-bedded, bioturbated, silty clays below, and commonly show an abrupt decrease in bed thickness and grain size above. The overlying overbank deposits are usually characterized by thin-bedded turbidites composed primarily of silt and clay. The sand beds constituting the Aqua HARP (Site 935), Brown HARP (Site 936), and Amazon HARP (Site 944) are organized into a single group of thick beds with no apparent bed-thickness trend, except perhaps for a slight thickening-upward trend at the base of the Brown HARP at Site 936 (Fig. 11B; 105–90 mbsf).

The rather sharp basal contact suggests that channel bifurcation occurs abruptly, as the levee of the parent channel is breached upslope. The presence of abundant mud clasts in the thicker sand beds within a HARP interval points to the erosive ability of these flows. Many of the clasts recovered in the cores and observed in the images are partly compacted (resistive in the images), suggesting that this material probably was buried and subsequently exhumed. This suggests that clasts were ripped from the substrate some distance upslope of the site of their final deposition, rather than being locally generated rip-up clasts. Obvious sources for such clasts are the places where levees are breached and eroded during channel bifurcation. There is evidence for significant channel entrenchment after bifurcation, in particular across the knickpoint introduced during channel bifurcation. Whether channel entrenchment extends headward for large distances is unknown.

The contrast in grain size observed across the upper boundary of the HARP units might indicate that the sediment load of turbidity currents changes abruptly to silts and clays as levees begin to develop. Pirmez (1994) argues that such a change in grain size may mark the completion of the final stages of adjustment of the longitudinal profile of the channel to its new post-avulsion course. After this adjustment is complete, the entrenchment and redistribution of those older coarse-grained channel-floor deposits that are upslope of the avulsion site would cease. External controls such as sea-level changes affecting the supply of sediment to the canyon might also account for the fining. Age dating shows, however, that channel switching occurs over a very short time interval, making it difficult to argue that lower frequency external forcing mechanisms like sea-level fluctuations control the supply of sediment to the fan.

The observation of a sharp downlap surface above the HARP unit is, in our view, key to the correct interpretation of the sharp grain-size change. Immediately after the bifurcation, flows are expected to follow the deepest axis of the interchannel low downslope of the avulsion site. After initial deposition of a 5- to 25-m-thick sandy unit, the topography may be sufficiently modified for subsequent sand-load flows to follow a different route, accounting for the observation that HARPs are in most cases formed of multiple lens-shaped units. At some point after bifurcation, however, the supply of sand is either diminished or becomes concentrated in a channel as levees begin to develop and extend down the fan. Extension and growth of the levees produces the sharp downlap surface, with overbank muds lying directly on sandy lenses.

HARP units have their sharpest tops on the middle fan (e.g., Site 936). Sand, which was initially carried in unconfined flows traveling down the interchannel low, presumably becomes concentrated at the channel axis and is carried farther downfan to be deposited at the channel mouth, where levee height diminishes. Directly in front of channels, aggrading channel-axis deposits forming areally restricted HARs are expected to lie immediately above the HARP unit, so the top of the HARP sands might not be so sharp as at Site 936. As an example, channel-axis sands overlie the HARP unit drilled at Site 945 (Shipboard Scientific Party, 1995h). Here, an 8-m-thick sand bed containing abundant, partly compacted mud clasts is interpreted to have been derived from upslope entrenchment of the channel after the 1C bifurcation (Pirmez and Flood, 1995; Flood, Piper, Klaus, et al., 1995). The top of the underlying HARP consists of an ~10-m-thick cluster of medium to very thick sand beds that thicken upward. Elsewhere on the fan, those rare sand-rich intervals that thicken upward through 10–20 m (e.g., Fig. 3D, 167–160 mbsf and 150–141 mbsf; Fig. 3E, 261–250 mbsf) may have formed the same way, by channel-mouth progradation as envisioned by Mutti and Ghibaudo (1972). In Hole 944A, 150–141 mbsf (Fig. 3D, back-pocket foldout), the thickening-upward interval correlates with activity of a small, unleveed channel that advanced over the Orange-1 system.

Deposits that formed at the mouths of small channels on the middle and lower fan are probably present throughout the Orange-1 Channel-levee System. The acoustically transparent overbank deposits of the Orange-1 system decrease in thickness significantly downslope of Site 936, and a relatively thin unit of discontinuous HARs overlying the Unit R MTD can be traced for long distances. Where this HARP was penetrated at Site 936 (Fig. 11B, 147–118 mbsf), some of the bed clusters show an apparent upward thickening (e.g., Fig. 3C, back-pocket foldout; 129–119 mbsf).

Within those HARP units that can be directly tied to a particular bifurcation, asymmetric trends in bed thickness are absent. Instead, sand beds are organized into packets (i.e., clusters) a few tens of meters thick. These packets generally have sharp basal contacts and fairly sharp tops; locally, the bases of packets are gradational. This type of organization appears to characterize the rapid onset of deposition, perhaps precipitated by an upslope avulsion, followed by rapid lateral switching of the depocenter to produce stacked sandy lenses. Thicker intervals of thin-bedded silty clays that commonly overlie these sand clusters probably are distal overbank deposits.

Pirmez and Flood (1995), comparing levee thicknesses across a bifurcation site, showed that the sand-loaded, post-avulsion flows are effectively confined to the channel so that they do not generate thick overbank deposits. This confinement may result from (1) an increase in channel relief due to downcutting, or (2) a decrease in flow thickness for the more sandy flows (Bowen et al., 1984; Normark and Piper, 1991). A combination of these two processes may occur. During initial headward entrenchment, the channel will deepen (mechanism 1, above), decreasing the potential for material in suspension to spill over the levees. Manley et al. (this volume) and Shipboard Scientific Party (1995e) show that sediment within the overbank succession coarsens at the onset of bifurcation, corresponding to reflections that terminate (downlap) closer to the channel axis. This observation indicates that overspill of small volumes of coarser sediment (silt and fine sand) continues to occur, in spite of entrenchment. The flows responsible for this coarser, more limited overspill may have been thinner than the silt/clay-rich flows that generated thick overbank deposits (mechanism 2, above).

Is the evidence for coarser, albeit limited, post-avulsion overspill, combined with the coarse and locally pebbly texture of HARP sands, sufficient grounds for concluding that there is a fundamental change in flow type during avulsion episodes? We cannot yet answer this

question, because the characteristics of the electrical facies that we observe in the sandiest HARPs are not considered by us to be diagnostic of particular flow processes. Clasts, locally with evidence for soft-sediment deformation and abundant sand matrix, might suggest that some of these sand beds were emplaced by liquefied flows or debris flows. However, many of the characteristics of these beds, in particular the apparent widespread development of normal size grading, can result from the final stages of deposition from the bases of high-density turbidity currents that were rolling mud clasts along the bed (Lowe, 1982; Kneller and Branney, 1995; Hiscott et al., in press).

Extrapolation of our observations on HARP lithofacies (Fig. 3, back-pocket foldout) to HARPs throughout the fan (Fig. 14, back-pocket foldout) indicates that the Amazon Fan contains sheets of sand with high sand to mud ratios that are tens of meters thick and several kilometers to several tens of kilometers in lateral extent. Other large submarine fans like the Indus Fan (Kolla and Macurda, 1988; McHargue, 1991), the Bengal Fan (Droz and Bellaiche, 1991), the Mississippi Fan (Weimer, 1990), and the Rhône Fan (Droz and Bellaiche, 1986; d'Heilly et al., 1988) also contain onlapping units at the base of channel-levee systems, with both high- and low-amplitude seismic character. By analogy with the Amazon Fan, these and other large fans may contain sand-rich units associated with channel bifurcations and with the distal ends of channels. The overbank muds both above and below the HARP sands may provide seals for stratigraphic hydrocarbon traps if such units become reservoirs.

HARP Stratigraphy Compared With Ancient Deep-Water Successions

A large number of ancient turbidite successions are characterized by alternations, on a scale of tens of meters, of (1) silt through mud turbidites, and (2) clusters of sandstone beds, called "packets" (Sullwold, 1960; Ojakangas, 1968; Nilsen and Simoni, 1973; "mega-sequences" of Ricci Lucchi, 1975; Hiscott, 1980; turbidite substages of Mutti and Normark, 1991; numerous papers in Pickering et al., 1995). These successions are classified as "mud/sand-rich systems" by Reading and Richards (1994), and contain as much as 70% sand in proximal areas.

Reading and Richards (1994) provide the following list of typical mud/sand-rich fan systems: Rhône Fan, Delgada Fan, La Jolla Fan, Navy Fan. It is these and similar fans that are generally perceived to be modern analogs for many ancient successions now preserved in orogenic belts (Normark et al., 1993). In contrast, very large mud-rich fans fed by major rivers and deposited on oceanic crust have been discounted as suitable analogs for ancient mud/sand-rich fans. They are generally believed to contain little sand except at their distal extremities (Shanmugam and Moiola, 1988; Reading and Richards, 1994).

The Amazon Fan is widely classified as an elongate, mud-rich fan (Stow et al., 1984; Shanmugam and Moiola, 1988; Pickering et al., 1989; Reading and Richards, 1994), yet the sandy character of bed-by-bed sections through HARP intervals (Fig. 3, back-pocket foldout) is comparable to many ancient turbidite successions in, for example, foreland basins. In Hole 946A, the sharp-based upper and lower sand and pebbly sand packets with abundant mud clasts (Fig. 3E, 127–90 mbsf and 261–219 mbsf, back-pocket foldout) probably correspond to broadly channelized sand bodies in outcrops (e.g., Hiscott and Devries, 1995; Drinkwater, 1995). Other less sharply based packets (e.g., Hole 931B in Fig. 3A, 162–152 mbsf; Hole 936A in Fig. 3C, 99–76 mbsf; Hole 946A in Fig. 3E, 212–199 mbsf, back-pocket foldout) are similar to ancient deposits that have been described as unchannelized, aggradational turbidite sheets (e.g., Cattaneo and Ricci Lucchi, 1995) or lobes (Mutti and Normark, 1987).

Bed-Thickness Statistics

The number of beds measured at some sites appears insufficient to constrain scaling exponents of bed-thickness distributions, under the assumption that the expected distribution of bed thicknesses follows a power law. The change in the scaling exponent, *B*, within the distribution of bed thicknesses in the global data set (Fig. 15E) may be related to (1) preferential erosion of thinner beds, (2) an observational bias toward thicker beds, and/or (3) different processes associated with the formation of beds of different thickness. Alternatives 1 and 2 are both based on an assumption that the expected distribution of bed thicknesses is a power law with a single exponent, with deviations from this model being the result of modifications to the original distribution by erosion or sampling error.

Alternative 1 implies that the kink at ~0.3–0.4 m is due to the preferential removal, by erosion, of beds thinner than this value. If the depth of erosion were to be random, the plots in log-log space (Fig. 15) should show a smooth curvature instead of a kink. Instead, the abrupt change in slope at T~0.35 m suggests that the depth of erosion was always quite shallow. Erosion at the base of sand beds is evident in the FMS images of many beds, and the occurrence of clasts in sand beds provides further evidence for erosion. However, the common presence of partially compacted clasts in sand beds suggests either that the overall depth of erosion by one or more flows was deeper than 0.35 m, or that the clasts were derived from an upslope locality so that they provide no constraints on the local depth of erosion at the drillsite.

By analyzing only the HARP units, we clearly biased the distribution of bed thicknesses by ignoring thick intervals of thin-bedded sediments associated with overbank deposits (alternative 2, above). Future analysis should include measurements in the levee deposits to see whether and how the predominantly thin-bedded silts and silty clays might change the overall bed-thickness distributions. We note that alternative 2 can only be considered because the data were gathered from a modern fan, where the regional topography and fan stratigraphy are fairly well known at each site. Such questions cannot, in general, be considered for ancient turbidite systems observed through limited outcrop windows; still, power-law distributions of bed thickness have been reported from such ancient fans (e.g., Rothman et al., 1994a).

It is possible that the thick sand beds containing mud clasts were generated by different flow processes than the thinner beds (alternative 3, above), leading to bed geometries intrinsically different from those of the thin beds. In particular, if the thicker beds were deposited by more concentrated and viscous flows, they might be expected to have a more limited extent, relative to the flow size, than the thinner beds. Leg 155 scientists actively discussed the possibility that thick sand beds with mud clasts might have been emplaced by liquefied flows or debris flows rather than by turbidity currents.

An alternative to Equation 1 that allows investigation of the issue of flow spreading is to assume that the distribution of bed volumes, rather than bed thicknesses, follows a power law (Alberto Malinverno, pers. comm., 1996); that is,

$$N\,(\text{volume} > V) \propto V^{-C}\,, \tag{2}$$

where c is a positive exponent. If we then follow Rothman et al. (1994a) and introduce an exponent ζ to scale deposit volume, V, to deposit area, S (i.e., $S \propto V^{\zeta}$), then the thickness scaling exponent, B, is related to the volume scaling exponent, ζ, by (Rothman et al., 1994b; Alberto Malinverno, pers. comm., 1996):

$$B = c/(1–\zeta), \text{ or } \zeta = (B–c)/B; \text{ for } 0 < \zeta \le 1. \tag{3}$$

The volume scaling exponent, ζ, is a measure of how widely the beds in a given sequence are spread laterally, relative to the deposit volume. The larger the value of ζ (and B), the more laterally spread are beds with greater volumes. For beds that are confined and therefore cover the same area regardless of the bed volume, $\zeta = 0$. ζ cannot realistically be negative, because $\zeta < 0$ in a single population of beds would dictate that beds become smaller in a surface area with

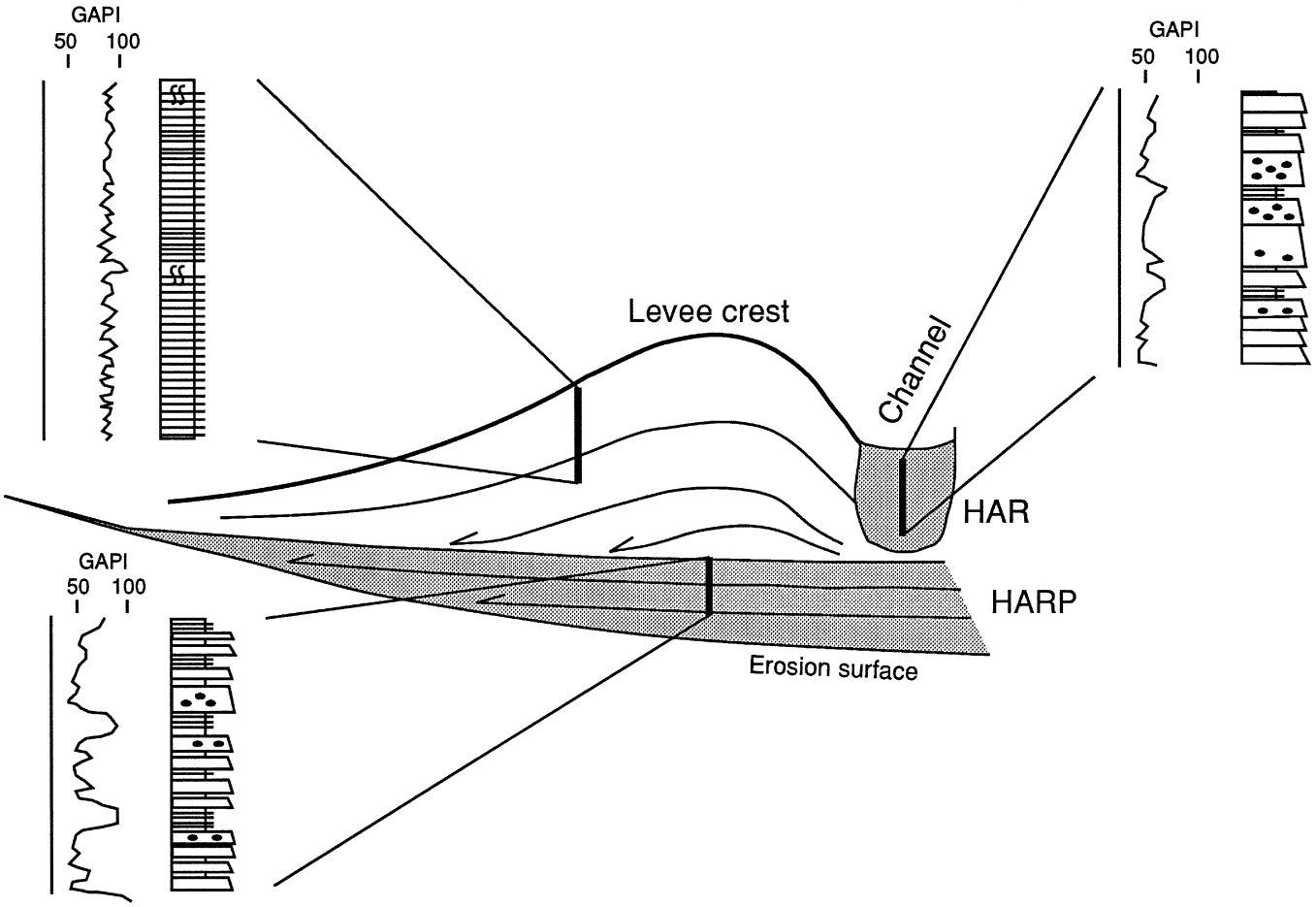

Figure 16. Summary of geometry, stratigraphy, lithofacies, and gamma-ray signature of components of Amazon Fan channel-levee systems, including a sheet-like sandy succession formed by redistribution of upfan channel-floor sands into an interchannel low following avulsion (HARP), downlapping mud/silt deposits of an aggrading levee, and aggrading channel-floor sands of the new channel segment (HAR). Each column represents ~30–50 m of section.

larger volume. Certainly sandy debris flows of large volume might cover less area than sandy turbidites of smaller volume, but these deposits would not likely all belong to the same bed-thickness population with the same scaling exponent.

From the global plot of bed thickness for the Amazon Fan (Fig. 15F), $B_{thin} = 0.4$ and $B_{thick} = 1.3$. If bed volumes are distributed according to a single power law with constant exponent c, then different values of B for thin and thick beds can result only if the thin beds are confined (e.g., $\zeta_{thin} = 0$; $c = B_{thin} = 0.4$) and thick beds are unconfined ($c = 0.4$; $B_{thick} = 1.3$; $\zeta_{thick} = 0.7$). At present, we cannot think of a compelling reason why thin-bedded turbidites within HARP intervals should have been unable to extend widely over the broad interchannel depressions downslope of avulsion sites. Neither is the notion that the thicker coarser beds could cover larger areas of the fan consistent with the view that these beds might have been deposited from less mobile, more viscous sediment gravity flows. It is primarily for these reasons that we tentatively reject the hypothesis that the bed volumes of HARP turbidites are distributed according to a power law with a constant exponent. Instead, we prefer to believe that, regardless of whether bed thickness or bed volume was initially distributed according to a power law, selective erosion of some of the beds thinner than ~0.35 m probably modified the original distribution (alternative 1, above). Further studies are needed, however, to decide whether bed thickness distributions reflect in any way the relative degree to which different facies spread away from channels and onto the interchannel lows. If flow confinement vs. flow spreading is an important controlling factor, then certain facies indeed may be characterized by different scaling factors (i.e., different B values).

CONCLUSIONS

Channel bifurcation on the Amazon Fan results in the abrupt supply of sand to topographic depressions (i.e., interchannel lows) between channel-levee systems. The sand units correspond to HARPs seen on the seismic reflection data, above an angular and erosional unconformity marking the onset of development of the channel-levee system (Fig. 16). The HARPs are composed of single sand beds up to 12 m thick and amalgamated beds >30 m thick. Many beds >1 m thick contain clasts. In cores, these consist of soft and partly compacted muds as well as lithified silts. The abundance of sand beds with clasts indicates that a significant fraction of material deposited within HARP units was remobilized from upslope channel deposits and eroded levees.

A channel bifurcation results in the formation of a knickpoint that will probably lead to flow acceleration, enhancing the erosive power of turbidity currents. Channel entrenchment and changes in channel sinuosity across and upslope of the bifurcation site will likely result in an increased supply of sand and clasts to the flows. Downslope of the bifurcation site, flows are relatively free to spread laterally, bounded only by the topographic highs of adjacent channel-levee systems.

On the Amazon Fan, the several sand packets within each HARP unit were deposited during single lowstands of sea level, so that the primary control on sand delivery to any site is probably autocyclic. The most likely processes, based on the study of Amazon Channel planform and gradients (Pirmez, 1994), are upfan avulsions and meander-loop cutoffs. Both these processes result in local channel en-

trenchment and transfer of sand and mud clasts farther down the fan to newly active interchannel lobes (HARPs) and lower fan lobes (e.g., Site 946). This sand mobilization is likely episodic (forming "packets") because entrenchment probably proceeds by piecemeal headward erosion in channel segments undergoing gradient changes. Periodic shifts in the position of focused sand deposition in the interchannel low also can lead to clustering of the thicker beds in the HARP unit.

In the middle fan, HARP units associated with individual bifurcations form 10- to 30 m-thick clusters that are sharply separated above and below from thin-bedded overbank deposits. On the lower fan, similar clusters appear to be stacked upon each other with little, if any, intervening overbank deposits, forming sand bodies up to 100 m thick. Where such sand bodies are overlain by an aggrading channel-axis deposit (HAR), total sand thickness may be even greater. In the mud-rich Amazon Fan, such sand bodies are encased in thin-bedded silts and silty clays that seal stratigraphic traps if the sand sheets eventually become a hydrocarbon reservoir.

Sharply bounded sand packets contrast with packets in which there is a gradual increase in bed thickness upward over intervals of 1–10 m. The sharp-based clusters are interpreted to result from upstream avulsion and abrupt lateral switching of the local fan depocenter. Clusters with a gradual increase in bed thickness at the base, in contrast, are interpreted to represent the advancement of channel-mouth deposits over more distal portions of the fan.

Scaling exponents of the power-law-distributed bed thicknesses within the fan are less than one for the thin to medium bedded turbidites and larger than one for the thick to very thick bedded intervals. A pronounced kink in the distribution at a thickness of 0.35 m may indicate that beds thinner and thicker than this value form by significantly different processes, possibly including different kinds of sediment gravity flows (e.g., thinner beds by overbank spill from channels and thicker beds by sheetflow downfan from avulsion sites). Alternatively, the fact that thin beds are less common than expected for a single power-law distribution may simply be the result of preferential erosion of some of the thinner beds.

An important and unexpected conclusion from our analysis of Leg 155 data is that the so-called mud-rich Amazon Fan, and presumably other large fans, contain widespread sheetlike units locally >100 m thick, indistinguishable in facies and sand content from many ancient mud/sand-rich successions described by field geologists. Although it remains true that some small California borderland fans are potentially good analogs for such ancient deposits, larger channel-levee–dominated systems, periodically supplying sand to interchannel depressions following avulsions, also need to be considered.

ACKNOWLEDGMENTS

This work was supported by JOI-USSSP grants to CP (155-20878b) and JK (155-20849b) and by a Natural Sciences and Engineering Research Council of Canada grant (OGP0006088) to RNH. Acquisition and processing of seismic reflection data were supported by NSF-OCE 82-14819 and JOI Inc. JSC1592. We thank the crew of *SEDCO-BP 471* (*JOIDES Resolution*) for the successful drilling of the Amazon Fan and the Leg 155 Shipboard Scientific Party, in particular, the members of the sedimentology team, for the detailed descriptions of cores that facilitated our detailed correlation with FMS images and logs. This is LDEO contribution #5508.

REFERENCES

Bouma, A.H., 1962. *Sedimentology of Some Flysch Deposits: A Graphic Approach to Facies Interpretation:* Amsterdam (Elsevier).

Bouma, A.H., Coleman, J.M., Meyer, A.W., et al., 1986. *Init. Repts. DSDP,* 96: Washington (U.S. Govt. Printing Office).

Bowen, D., Normark, W.N., and Piper, D.J.W., 1984. Modelling turbidity currents on Navy submarine fan, California Continental Borderland. *Sedimentology,* 31:169–185.

Carneiro de Castro, J., Miura, K., and Estrela-Braga, J.A., 1978. Stratigraphic and structural framework of the Foz do Amazonas Basin. *Proc. Annu. Offshore Technol. Conf*., 3:1843–1848.

Cattaneo, A., and Ricci Lucchi, F., 1995. Long-distance correlation of sandy turbidites: a 2.5 km long cross-section of Marnoso-arenacea, Santerno Valley, northern Apennines. *In* Pickering, K.T., Hiscott, R.N., Kenyon, N.H., Ricci Lucchi, F., and Smith, R.D.A. (Eds.), *Atlas of Deep Water Environments: Architectural Style in Turbidite Systems:* London (Chapman and Hall), 303–306.

Cochran, J.R., Stow, D.A.V., Auroux, C., et al., 1989. *Proc. ODP, Init. Repts.,* 116: College Station, TX (Ocean Drilling Program).

Damuth, J.E., Flood, R.D., Kowsmann, R.O., Belderson, R.H., and Gorini, M.A., 1988. Anatomy and growth pattern of Amazon deep-sea fan as revealed by long-range side-scan sonar (GLORIA) and high-resolution seismic studies. *AAPG Bull.,* 72:885–911.

Damuth, J.E., Kolla, V., Flood, R.D., Kowsmann, R.O., Monteiro, M.C., Gorini, M.A., Palma, J.J.C., and Belderson, R.H., 1983a. Distributary channel meandering and bifurcation patterns on Amazon deep-sea fan as revealed by long-range side-scan sonar (GLORIA). *Geology,* 11:94–98.

Damuth, J.E., Kowsmann, R.O., Flood, R.D., Belderson, R.H., and Gorini, M.A., 1983b. Age relationships of distributary channels on Amazon deep-sea fan: implications for fan growth pattern. *Geology,* 11:470–473.

d'Heilly, P., Millot, C., Monaco, A., and Got, H., 1988. Hydrodynamic study of the furrow of the Petit-Rhône canyon. *Deep-Sea Res. Part A,* 35:465–471.

Drinkwater, N.J., 1995. Sheet-like turbidite system: the Kongsfjord Formation, Finnmark, north Norway. *In* Pickering, K.T., Hiscott, R.N., Kenyon, N.H., Ricci Lucchi, F., and Smith, R.D.A. (Eds.), *Atlas of Deep Water Environments: Architectural Style in Turbidite Systems:* London (Chapman and Hall), 267–274.

Droz, L., and Bellaiche, G., 1985. Rhône deep-sea fan: morphostructure and growth pattern. *AAPG Bull.,* 69:460–479.

————, 1991. Seismic facies and geologic evolution of the central portion of the Indus Fan. *In* Weimer, P., and Link, M.H. (Eds.), *Seismic Facies and Sedimentary Processes of Modern and Ancient Submarine Fans:* New York (Springer-Verlag), 383–402.

Droz, L., Rigaut, F., Cochonat, P., and Tofani, R., 1996. Morphology and recent sedimentary evolution of the Zaire turbidite system (Gulf of Guinea). *Geol. Soc. Am. Bull.,* 108:253–269.

Flood, R.D., 1987. Side echoes from a sinuous fan channel obscure the structure of submarine fan channel/levee systems, Amazon Fan. *Geo-Mar. Lett.,* 7:15–22.

Flood, R.D., Piper, D.J.W., and Shipboard Scientific Party, 1995. Introduction. *In* Flood, R.D., Piper, D.J.W., Klaus, A., et al., *Proc. ODP, Init. Repts.,* 155: College Station, TX (Ocean Drilling Program), 5–16.

Flood, R.D., Manley, P.L., Kowsmann, R.O., Appi, C.J., and Pirmez, C., 1991. Seismic facies and late Quaternary growth of Amazon submarine fan. *In* Weimer, P., and Link, M.H. (Eds.), *Seismic Facies and Sedimentary Processes of Submarine Fans and Turbidite Systems:* New York (Springer), 415–433.

Flood, R.D., Piper, D.J.W., Klaus, A., et al., 1995. *Proc. ODP, Init. Repts.,* 155: College Station, TX (Ocean Drilling Program).

Hiscott, R.N., 1980. Depositional framework of sandy mid-fan complexes of Tourelle Formation, Ordovician, Quebec. *AAPG Bull.,* 64:1052–1077.

Hiscott, R.N., Colella, A., Pezard, P., Lovell, M.A., and Malinverno, A., 1992. Sedimentology of deep-water volcaniclastics, Oligocene Izu-Bonin forearc basin, based on formation microscanner images. *In* Taylor, B., Fujioka, K., et al., *Proc. ODP, Sci. Results,* 126: College Station, TX (Ocean Drilling Program), 75–96.

Hiscott, R.N., and Devries, M., 1995. Internal characteristics of sandbodies of the Ordovician Tourelle Formation, Quebec, Canada. *In* Pickering, K.T., Hiscott, R.N., Kenyon, N.H., Ricci Lucchi, F., and Smith, R.D.A. (Eds.), *Atlas of Deep Water Environments: Architectural Style in Turbidite Systems:* London (Chapman and Hall), 207–211.

Hiscott, R.N., Pickering, K.T., Bouma, A.H., Hand, B.M., Kneller, B.C., Postma, G., and Soh, W., in press. Basin-floor fans in the North Sea: sequence stratigraphic models vs. sedimentary facies: Discussion. *AAPG Bull.*

Kneller, B.C., and Branney, M.J., 1995. Sustained high-density turbidity currents and the deposition of thick massive sands. *Sedimentology,* 42:607–616.

Kolla, V., and Macurda, D.B., 1988. Sea-level changes and the timing of turbidity: current events in deep-sea fan sediments. *In* Wilgus, C.K., Hastings, B.S., Kendall, C.G., Posamentier, H.W., Ross, C.A., and Van Wagoner, J.C. (Eds.), *Sea-Level Changes: An Integrated Approach*. Spec. Publ.—Soc. Econ. Paleontol. Mineral., 42:125–154.

Lowe, D.R., 1982. Sediment gravity flows: II. Depositional models with special reference to the deposits of high-density turbidity currents. *J. Sediment. Petrol.*, 52:279–297.
Manley, P.L., and Flood, R.D., 1988. Cyclic sediment deposition within Amazon deep-sea fan. *AAPG Bull.*, 72:912–925.
McHargue, T.R., 1991. Seismic facies, processes, and evolution of Miocene inner fan channels, Indus Submarine Fan. *In* Weimer, P., and Link, M.H. (Eds.), *Seismic Facies and Sedimentary Processes of Modern and Ancient Submarine Fans:* New York (Springer-Verlag), 403–414.
Mutti, E., and Ghibaudo, G., 1972. Un esempio di torbiditi di conoide sottomarina esterna: le Arenarie di San Salvatore (Formazione di Bobbio, Miocene) nell'Appennino di Piacenza. *Mem. Acc. Sci. Torino Classe Sci. Fis. Nat.*, Ser. 4, 16.
Mutti, E., and Normark, W.R., 1987. Comparing examples of modern and ancient turbidite systems: problems and concepts. *In* Leggett, J.K., and Zuffa, G.G. (Eds.), *Marine Clastic Sedimentology:* London (Graham & Trotman), 1–38.
————, 1991. An integrated approach to the study of turbidite systems. *In* Weimer, P., and Link, M.H. (Eds.), *Seismic Facies and Sedimentary Processes of Modern and Ancient Submarine Fans:* New York (Springer-Verlag), 75–106.
Nilsen, T.H., and Simoni, T.R., Jr., 1973. Deep-sea fan paleocurrent patterns of the Eocene Butano Sandstone, Santa Cruz Mountains, California. *J. Res. U.S. Geol. Surv.*, 1:439–452.
Normark, W.R., and Piper, D.J.W., 1991. Initiation processes and flow evolution of turbidity currents: implications for the depositional record. *In* Osborne, R.H. (Ed.), *From Shoreline to Abyss: Contributions to Marine Geology in Honor of Francis Parker Shepard.* Spec. Publ.—Soc. Econ. Paleontol. Mineral., 46:207–230.
Normark, W.R., Posamentier, H.W., and Mutti, E., 1993. Submarine turbidite systems: state of the art and future directions. *Rev. Geophys.*, 31:91–116.
Ojakangas, R.W., 1968. Cretaceous sedimentation, Sacramento Valley, California. *Geol. Soc. Am. Bull.*, 79:973–1008.
Pickering, K.T., Hiscott, R., and Hein, F.J., 1989. *Deep-marine Environments: Clastic Sedimentation and Tectonics:* London (Unwin Hyman).
Pickering, K.T., Hiscott, R.N., Kenyon, N.H., Ricci Lucchi, F., and Smith, R.D.A. (Eds.), 1995. *Atlas of Deep Water Environments: Architectural Style in Turbidite Systems:* London (Chapman and Hall).
Pirmez, C., 1994. Growth of a submarine meandering channel-levee system on the Amazon Fan [Ph.D. thesis]. Columbia Univ., New York.
Pirmez, C., Breen, N.A., Flood, R.D., O'Connell, S., Jacobi, R., Ladd, J.W., Westbrook, G., Franco, J.V., Garzon, M., and Arias-Isaza, F. 1990. A GLORIA mosiac of the Magdalena Deep-Sea Fan, Northern Colombian Convergent Margin. *AAPG* Ann. Conv. Off. Prog., 153.
Pirmez, C., and Flood, R.D., 1995. Morphology and structure of Amazon Channel. *In* Flood, R.D., Piper, D.J.W., Klaus, A., et al., *Proc. ODP, Init. Repts.*, 155: College Station, TX (Ocean Drilling Program), 23–45.
Pratson, E., Pirmez, C., and Goldberg, D., 1995. A refinement of Formation MicroScanner depth shifting in the Ocean Drilling Program (ODP). *Eos* 76:F326.
Reading, H.G., and Richards, M., 1994. Turbidite systems in deep-water basin margins classified by grain size and feeder system. *AAPG Bull.*, 78:792–822.
Ricci Lucchi, F., 1975. Depositional cycles in two turbidite formations of the Northern Apennines, Italy. *J. Sediment. Petrol.*, 45:3–43.
Rothman, D.H., Grotzinger, J.P., and Flemings, P.B., 1994a. Scaling in turbidite deposition. *J. Sediment. Res.*, 64A:59–67.
————, 1994b. Scaling in turbidite deposition, Reply. *J. Sediment. Res.*, 64A:934.
Schlumberger, 1989. *Log Interpretation Principles/Applications:* Houston, TX (Schlumberger Educ. Services).
Serra, O., 1989. *Formation MicroScanner Image Interpretation:* Houston (Schlumberger Educ. Services), SMP-7028.
Shanmugan, G., and Moiola, R.J., 1988. Submarine fans: characteristics, models, classification, and reservoir potential. *Earth-Sci. Rev.*, 24:383–428.
Shipboard Scientific Party, 1995a. Leg synthesis. *In* Flood, R.D., Piper, D.J.W., Klaus, A., et al., *Proc. ODP, Init. Repts.*, 155: College Station, TX (Ocean Drilling Program), 17–21.
————, 1995b. Site 931. *In* Flood, R.D., Piper, D.J.W., Klaus, A., et al., *Proc. ODP, Init. Repts.*, 155: College Station, TX (Ocean Drilling Program), 123–164.
————, 1995c. Site 935. *In* Flood, R.D., Piper, D.J.W., Klaus, A., et al., *Proc. ODP, Init. Repts.*, 155: College Station, TX (Ocean Drilling Program), 273–319.
————, 1995d. Site 936. *In* Flood, R.D., Piper, D.J.W., Klaus, A., et al., *Proc. ODP, Init. Repts.*, 155: College Station, TX (Ocean Drilling Program), 321–382.
————, 1995e. Site 940. *In* Flood, R.D., Piper, D.J.W., Klaus, A., et al., *Proc. ODP, Init. Repts.*, 155: College Station, TX (Ocean Drilling Program), 463–501.
————, 1995f. Site 943. *In* Flood, R.D., Piper, D.J.W., Klaus, A., et al., *Proc. ODP, Init. Repts.*, 155: College Station, TX (Ocean Drilling Program), 569–589.
————, 1995g. Site 944. *In* Flood, R.D., Piper, D.J.W., Klaus, A., et al., *Proc. ODP, Init. Repts.*, 155: College Station, TX (Ocean Drilling Program), 591–633.
————, 1995h. Site 945. *In* Flood, R.D., Piper, D.J.W., Klaus, A., et al., *Proc. ODP, Init. Repts.*, 155: College Station, TX (Ocean Drilling Program), 635–655.
————, 1995i. Site 946. *In* Flood, R.D., Piper, D.J.W., Klaus, A., et al., *Proc. ODP, Init. Repts.*, 155: College Station, TX (Ocean Drilling Program), 657–693.
Stow, D.A.V., Howell, D.G., Nelson, C.H., 1984. Sedimentary, tectonic and sea level controls on submarine fan and slope-apron turbidite systems. *Geo-Mar. Lett.*, 3:57–64.
Sullwold, H.H., Jr., 1960. Tarzana fan, deep submarine fan of late Miocene age, Los Angeles County, California. *AAPG Bull.*, 44:433–457.
Weimer, P., 1990. Sequence stratigraphy, seismic geometries and depositional history of the Mississippi Fan, deep Gulf of Mexico. *AAPG Bull.*, 74:425–453.

Date of initial receipt: 18 December 1995
Date of acceptance: 3 May 1996
Ms 155SR-201

Previous Chapter Table of Contents Next Chapter